UNIVERSITY OF GHANA

COLLEGE OF BASIC AND APPLIED SCIENCES

DESIGN AND FABRICATION OF A TURNABLE SYSTEM FOR DOSIMETRY INVESTIGATION ON A COBALT-60 TOMOTHERAPY TREATMENT SYSTEM

BY

EUNICE ARTHUR

(10598729)

THIS THESIS IS SUBMITTED TO THE UNIVERSITY OF GHANA, LEGON IN PARTIAL FULFILMENT OF THE REQUIREMENT FOR THE AWARD OF MPHIL MEDICAL PHYSICS DEGREE

JULY 2018

DECLARATION

This thesis is the result of research work carried out by Eunice Arthur in the Department of Medical Physics, School of Nuclear and Allied Sciences, University of Ghana, under the supervision of Dr. Francis Hasford, Mr. Eric Kotei Addison and Mr. S.N. Tagoe

I hereby affirm that, no part of this work has been presented in part or whole to any other University or institution for the award of a diploma, or degree at any level. Accordingly, other works and/or researches done by other researchers cited in this work have been acknowledged under references.

……	……
EUNICE ARTHUR	DR. FRANCIS HASFORD
(STUDENT)	(PRINCIPAL SUPERVISOR)
Date……	Date……
……	……
MR. ERIC KOTEI ADDISON	MR. S.N. TAGOE
(CO-SUPERVISOR)	(CO-SUPERVISOR)
Date……	Date……

DEDICATION

This work is dedicated to my dear sister Harriet Asante and Uncle Edward Osei of blessed memory and to my entire family.

ACKNOWLEDGEMENTS

I wish to express my profound gratitude to ALMIGHT GOD for His Uncommon Favor upon my life. My sincere appreciation goes to Mr. Eric K.T. Addison, the Head of medical physics unit of the Komfo Anokye Teaching Hospital (KATH), Oncology Directorate and one of my supervisors; I have seen your sacrifices, financial support and struggles toward the experimental methods set for this thesis work. Dr. Francis Hasford, the Head of the Department of Medical Physic and my supervisor you cannot be left out; your guidance, patience, suggestions, financial support and encouragement has also been a great pathfinder; you are forever blessed. My sincere appreciation also goes to my supervisor Mr. N Tagoe and Prof. A.W.K. Kyere, the former Head of the Department of Medical Physics, for their valuable, guidance, contributions, encouragement and patience.

Furthermore, my sincere gratitude goes to Mr. Asare Van-Dycke of department of physics (KNUST) for his immense support and technical guidance in the fabrication of the turn table. Also, I would like to thank Mr. Alex Kwame Appiah of Suame Magazine for helping me attain the fabrication of the turn table. Miss Naa Momoede Quaye Abigail for her huge support and guidance in my day-to-day activity in the hospital where she played a key role in my practical work and experimental data collection. I am also thankful to the Oncology Directorate, KATH and to all the Senior Medical Physicists particularly Mr. Adom Joseph, radiation therapists, the national service personnels of 2017/2018 and to the Medical Physics Interns, especially Mr. Akosah Kingsley and Miss Olivia Adu- Poku, I am in-debated to you for all your support and I appreciate all our time together, advises and for their immense support during my data collection. My sister from another mother Annete Agyabeng I cannot pen down all your assistance Don sang saranghaeo!

TABLE OF CONTENT

LIST OF FIGURES

LIST OF TABLES

ABBREVIATIONS

WHO	World Health Organization
DNA	Deoxyribonucleic Acid
EBRT	Beam Radiation Therapy
3DCRT	Three-Dimensional Conformal Radiation Therapy
IMRT	Intensity Modulated Radiation Therapy
MLC	Multi Leaf Collimator
VMAT	Volumetric Arc Therapy
IGRT	Image Guided Radiation Therapy
CT	Computed Tomotherapy
LINACS	Linear Accelerators
Co-60	Cobalt -60 Teletherapy Unit
KATH	Komfo Anokye Teaching Hospital
CCSEO	Cancer Center of Southeastern Ontario
OAR	Organ at Risk
DTA	Distance to Agreement
TLDs	Thermo luminesce Dosimeter
QA	Quality of Assurance
OF	Output factor
TAR	Tissue Air Ratio

LIST OF SYMBOLS

Bs	Ambient pressure
Ci	Curie
Gy	Gray
K	Mean of readings
TPS	Treatment planning system
M	Mass
M_w	Mean check source measurements
nC	Nano coulomb
$N_{D,W}$	Estimated uncertainty reference value
P	Measured average atmospheric pressure
$Q_{measured}$	Measured check source value
R.H.	Relative humidity
T	Measured average temperature
V	Voltage
Z	Atomic number of an element
F	Beam Flatness
S	Beam symmetry
^oC	Degree Celsius
$_5D_w$	Absorbed dose to water rate
D_{max}	Maximum dose
D_{min}	Minimum dose

ABSTRACT

The objective of this research is to ascertain if it is feasible to replicate tomotherapy treatment with telecobalt machine based on phantom studies. To replicate gantry motion around a patient during tomotherapy treatment, the phantom was placed on a fabricated turn-table capable of translational and rotational motions while the gantry of the telecobalt machine was kept constant. The treatment simulations were performed with Cirus cobalt 60 teletherapy machine at the Komfo Anokye Teaching Hospital. The fabricated turn-table was made of a metal steel connected to wiper motors of 22, 35 and 50 rpm to control the translational and rotational motion of water phantom. The Co-60 beam dosimetric characteristics such as beam flatness beam, symmetry beam profile, tissue air ratio, output factors and percentage depth dose were determined with tomotherapy procedure. Measurements were done at source -to -surface distance of 80cm for tomotherapy beam using a Farmer type ionization chamber connected to a UNIDOS electrometer and 30 x 30cm^2 water phantom. Measurements were carried out using various field sizes ranged from 4x4 to 30x 30 cm^{2}at depths of 0.5cm, 5cm, 15cm and 20cm. The percentage depth dose increased from the surface to a depth of maximum dose which is 0.5cm for cobalt and decreased as the depth increased It was found that as field size increased the output factor and tissues air ratio increased due to an increased in scatter which increased the dose and decreased as depth increased. The beam flatness and beam symmetry were found to be 0.60 %, and 1.19% (at depth 10cm and width of 3cm from the central axis; and 0.74% at depth 5cm and width of 2 cm from the central axis) which agreed with the International Electrotechnical commission range of 3% and 2% respectively. The fabricated turn table

needs refinement in term of high rpm rotational motor to rotate fully-filled 30x30cm^2 water phantom and potentiometer to regulate the speed of the rotational motor.

CHAPTER ONE

INTRODUCTION

1.1 Background

Cancer is the abnormal proliferation of cells within the human body, which can occur at any part of the body and has the tendency of infiltrating into other neighboring tissues or spreading to other parts of the body. The spread of cancerous cells from their primary sites to other parts of the body is referred to as metastasis, and if this process is not curtailed may result in the death of an individual. Cancer is among the major causes of deaths in the world, with more than two thirds of cancer mortality occurring in low- and middle-income countries (WHO 2006). The common treatment modalities which are used in the management of cancer are: surgery; for the bulk removal of the tumor, chemotherapy; administering cytotoxic drugs (or antineoplastic) to destroy and or retard the growth of cancerous cells, and radiotherapy; using ionizing radiations to destroy cancerous cells (Tobias, 1992). Radiotherapy has been found to be very effective in the management of cancer, and more effective if combined with any of the other stipulated treatment modalities (Podgorsak, 2005; Van Dyk 1999). There are two mainstay methods of delivering radiation to a patient, which are external beam radiotherapy (EBRT) and Brachytherapy (IAEA 2003). During EBRT the radiation source is placed remote from the patient and collimation systems are used to propagate the radiation beam onto the patient. For Brachytherapy the radiation source is placed into the tumor or in closed proximity to it. It is estimated that about 52 to 60% of patients requiring treatment for cancer will be treated with radiotherapy (Schreiner, 2006; Foroudi et al., 2003). And out of this number of patients, 90% will receive EBRT (Schreiner, 2006)

Radiotherapy may be used for curative or palliative intent. Palliative intent when cure is not achievable, and the objective is for pain relief. Radiotherapy involves the use of directly ionizing radiation or indirectly ionizing radiation megavoltage beams, which when administered cause-damage to the deoxyribonucleic acid (DNA) of cell; genetic material of cells (Hall,2000). Photon beams are usually used for EBRT. The biological damage mechanism is associated with the breaking down of bonds in the DNA by photon beams in the presence of oxygen. The DNA is then damaged, and the cell cannot divide, or the damaged cell may be sufficient to reduce apoptosis in this process, water molecules are ionized to produce free radicals ($^{+}$ H or $^{-}$ H) which then interact with the DNA to sustain the cell killing mechanism, there by destroying the tumor; the process is very feasible in the human body since the body contains approximately 70% of water (Hall 2000). With reference to the cell killing of radiation, there is the possibility of also causing significant damage to normal tissues.

Owing to the adverse effects of radiation on tissues, it is therefore important to find ways of realizing the intent of treatment prior to treatment delivery during EBRT. This will be crucial in the optimization of radiation doses to the intended target volume to achieve the principal objective of radiotherapy. The main objective of radiotherapy is to deliver maximum dose to the tumor while at the same time reducing doses as much as reasonably achievable to normal healthy tissues close to the tumor. Radiation dose optimization in EBRT is influenced by a lot of factors such as: patient anatomical irregularities, non-availability of appropriate treatment machines and treatment modality used to deliver the radiation. Also, the dose distribution within a patient has been found to be the most reliable quantity that links treatment parameters of any radiotherapy treatment technique to

treatment outcome. Therefore, achieving favorable treatment outcomes is dependent on how best we can optimize the radiation dose to our intended target. It is also imperative that we know with very high level of accuracy the magnitude of the radiation dose that will be deposited at any point within the patient during EBRT. Since it is impossible to place radiation detectors within a patient, the dose distribution within the patient is calculated. Dosimetric functions and or beam data acquired in a water phantom with suitable detectors are used to link doses measured in the water phantom to what will be pertaining within a patient. The dose estimation process within a patient is now a preserve of specialized computers known as treatment planning systems (TPSs) owing to the complexities involved with the dose calculation processes. The TPS is also used as dose optimization tool, which helps the user to select optimal irradiation geometries to produce desired dose distributions within a patient base on try and error approach. Choice of irradiation geometries or treatment technique to give optimal treatment outcome is therefore paramount to EBRT. During EBRT, it is also a requirement that the dose distribution within the target volume must be uniform and should conform to the shape of the target volume as much as possible. Various EBRT treatment techniques had been introduced to facilitate the attainment of the stated requirements. Conventional EBRT technique uses static multiple beams with appropriate field shaping coming from different directions of the patient to achieve the stated objective. This is the so-called three-dimensional (3-D) conformal radiation therapy (3DCRT) (Ezzell et al:2003Purdy and Starkschall 1999); Delivery of the radiation over a wide area of the patient minimizes radiation doses to healthy normal tissues. 3DCRT has limitations with dose coverage for tumors that assumes concave shapes and sparing critical tissues within the concavity is problematic. Also, since

a tumor may have different concentration of cancerous cells, there is the need to escalate radiation doses to certain areas of the tumor, specifically regions with high concentration of cancerous cells. For 3DCRT, dose escalation is achieved by treating the patient in phases with different irradiation geometries. With this approach, limiting doses to organs at risk (OARs) is a daunting task, and usually the intent of treatment will not be realized if the patient default treatment. However due to technological advancements in computer hardware and software capabilities and the introduction of computers into radiotherapy, an advanced form of 3DCRT had been introduced to address issues with the conventional 3DCRT. The advanced 3DCRT uses beams with modulated fluence distributions across a beam to treat a patient (Webb2003; Ezell et al, 2003). In this way dose escalation can be achieved in a single fraction of the entire treatment session. This form of 3DCRT is referred to as intensity modulated radiotherapy (IMRT). For effective implementation of IMRT, the conventional teletherapy machine (usually a linear accelerator) is adapted and fitted with a tertiary collimator system known as multi–leaf collimator (MLC). The collimator consists of two opposing banks of interlocking thin width leaves (made of high atomic number material, such as tungsten or Tantalum), which are automated to move independently of each other. During treatment delivery the various leaves of the MLC are swept across a beam to modulate the intensity of radiation within the beam based on pre-defined dose distributions determined during inverse planning with a treatment planning system. This gives better tumor dose conformity, dose homogeneity and normal-tissue sparing compared to the conventional 3DCRT. Organ motion is non-trivial issue affecting doses received by organs during this treatment modality. To surmount dosimetric issues associated with organ motion during treatment delivery, gating and motion tracking

devices have been employed to monitor motions of organs, and to prompt the teletherapy machine to deliver radiation during prolong motion phase of a targeted organ. This type of treatment modality is referred to as image guided radiotherapy (IGRT). The duration for this type of treatment technique is prolonged and may not be feasible for treatment of tumors that span over a wide area.

The number of beams used in the treatment of a patient during EBRT is sometimes considered to be infinite, since improvements in dose conformity, dose homogeneity and normal-tissue sparing are dependent on the number of beams used and their orientations (directed angles relative the patient). With reference to this, tomotherapy based on the principle of computed tomography (CT) was developed and used for clinical applications (Mackie et al; 2006). For tomotherapy, the diagnostic x-ray tube of the CT is replaced with a megavoltage linear accelerator which continually moves around the patient during treatment. The patient is therefore treated with modulated fan-like beams. The beam modulation is achieved with miniaturized MLCs, which either open or close during treatment delivery. Volumetric arc therapy (VMAT) is an IMRT technique executed with linear accelerators (linacs) to replicate treatment with tomotherapy.

Set of beam data and or dosimetric functions are needed for effective implementation of the treatment technique. Beam data requirement is dependent on the complexity of the technique.

1.2 PROBLEM STATEMENT

The basic goal of radiotherapy treatment is the irradiation of a target volume whilst reducing the amount of radiation absorbed by healthy tissues. The modality used during

treatment is an important way of achieving this goal and tomotherapy is one of the modality that can be used. Tomotherapy is mostly performed on linear accelerators (LINAC) due to some of its beam characteristics. This study is therefore undertaken to find ways of adapting a telecobalt machine to make it possible to replicate tomotherapy treatment by designing and fabricating a turntable and finding the influence tomotherapy approach will have on beam characteristics of the telecobalt machine.

1.3 OBJECTIVES

The principal objective of this research is to design and fabricate a turntable to asses the feasibility of delivering tomotherapy with a conventional tele cobalt machine

Specific objectives of this research work are:

1. Using the constructed turntable, the basic dosimetric functions and beam data necessary to facilitate the implementation of tomotherapy with a Cirus cobalt 60 teletherapy machine.
2. To make appropriate recommendations from the findings.

1.4 RELEVANCE AND JUSTIFICATION

In radiotherapy the accurate delivery of radiation to organs while reducing the dose to normal tissues depends on the treatment modality used. There are various modalities to achieve this and tomotherapy is one of them. Tomotherapy is usually performed on Linacs machines; despite its advantages it has limited universal use because of its complex design and cost incur by patient during treatment by linacs, Due to this there is a limitation in the demand in developing countries. Ghana still utilize conventional radiation therapy machines such as Co-60 unit which is cheaper. The findings of this work will help the

Radiotherapy Centre develop confidence in the radiation treatment they offer to patients by comparing it with the tomotherapy procedures.

1.5 SCOPE AND LIMITATION

This research was performed on Cirus Cobalt-60 unit at the Oncology Directorate of the Komfo Anokye Teaching Hospital. In this research work, dosimetry equipment such as ionization chamber and electrometer were used to determine dosimetric parameters of the fabricated turn-table in tomotherapy procedure.

1.6 ORGANIZATION OF THESIS

The thesis is organized as follows: The first chapter deals with the introduction of the concept of study which covers the background of the study, problem statement and objectives. The second chapter deals with the literature review on the subject area. Third chapter focuses on materials and methods used to solve the study problem. The results obtained are presented and discussed in chapter four. Chapter five of the thesis deals with conclusions and recommendations are.

CHAPTER TWO

LITERATURE REVIEW

2.0 INTRODUCTION

The past years have witnessed a lot of development and improvement in Radiotherapy treatment delivery due to technological advancements in treatment machines. Many of these are geared towards advancement in beam-shaping devices, imaging systems, treatment planning systems, and dose calculation algorithms. Owing to the technological advancements, new treatment modalities had been introduced for clinical application. One of such treatment modality is IMRT, which allows clinicians to sculpture radiation doses to conform to the shape of a target volume and spare normal tissues from receiving significant amount of radiation dose. Inspired by the clinical benefits of IMRT which are mostly implemented with linacs, researchers are trying to find ways of implementing IMRT with telecobalt machines (Schreiner,2006). Other treatment modalities (or techniques) are discussed in this chapter as well as details of IMRT also being presented.

2.1.1 Conformal Radiotherapy

Conformal radiation therapy uses radiation beams that are shaped to conform to the shape of a target volume in the projection of a beam onto a plane perpendicular to the direction of propagation of the beam (Gadza and Coia, 2004). The area covered by a radiation is defined as field size and must be determined dosimetrically rather than using geometrical approach.

For effective implementation of conformal radiotherapy, axial CT images of the part of the patient to be treated are acquired and uploaded into a TPS for treatment simulation processes. The TPS reconstructs the patient from the CT data sets to obtain three-dimensional representation of the patient. Organ segmentation process is then carried out to allow easy identification of the target volume and OARs. Using the TPS, beams from a virtual treatment machine (like the one to be used in treating the patient) are selected for the treatment of the patient. Irradiation geometries are selected based on desired dose distributions obtained within the patient. The next element is the positioning of the radiation beams in 3D spaces to match optimally the beams to the shape the target, to decrease the treated volume, and to keep doses to OAR within limits. This is achieved using blocked beams and non-coplanar. The third element is to set a higher dose to the target wherever possible. There is a proof that escalation of dose can be applied without extreme injury, but clinical trials are required to demonstrate what clinical improvement can be achieved (Williams and Thwaites, 1993). Conformal radiotherapy allows the delivery of a radical doses to target volumes and concurrently reducing doses to normal healthy tissues during radiotherapy to minimizing the side-effects of treatment. The treatment process is quite cumbersome and most intended for patients whom undergoing curative radiotherapy. For palliative radiotherapy purpose the prescribe total doses are generally lesser and the effects of palliative radiotherapy are thus expected to be less; because conformal radiotherapy is not frequently used when delivering palliative treatment, though it is often desirable to minimize the volume of non-target tissue that is irradiated (IAEA TECDOC-1588, 2008).

2.1.2 Intensity Modulated Radiotherapy (IMRT)

Dose escalation to certain portions of the tumor volume is dicey with conformal radiotherapy and conforming the dose distribution to the shape of the target volume with conformal radiotherapy may be problematic for some situations. The spatial distribution of radiation dose within a patient is influenced by a lot of factors: such as patient skin contour and tissue inhomogeneities within the irradiated region. These couple with the often-complex shapes of tumors calls for the treatment of a patient with intensity modulated beams rather than using beams from conventional teletherapy machine with uniform intensity across a beam. This has led to the introduction of IMRT, where extensively intensity modulated beams are used for treatment (Xing et al., 2006). There are three types of IMRT, which depend on the procedure use to achieve the beam intensity modulation. They are compensator-based IMRT, collimator-based IMRT and MLC-based IMRT. Compensator-based IMRT uses compensating filters to modulate the beam intensity based on beam intensity map information generated with a TPS an advancement of conformal therapy, permits the shaping of radiation beam intensity. For collimator-based IMRT, the field for the beam is segmented into smaller fields and each segmented field is weighted differently. The segmented fields are formed with the normal collimator system of the teletherapy machine. In this way the resultant beams intended for the treat of the patient are modulated. For the later, intensity modulations are achieved with computer-controlled movement of leaves of the MLC during treatment delivery (Gadza and Coia, 2004). There are also two variants of MLC-based IMRT, which are static and dynamic MLC-based IMRTs. For the static MLC-based IMRT, each leaf sequence is followed by irradiation, which is referred step-and-shoot IMRT approach. For the dynamic MLC-based IMRT, the

beam is continuous on with the leaves movements–IMRT is now becoming the most favoured treatment choice for most radiotherapy facilities.

2.1.3 Image Guided Radiotherapy (IGRT)

Image guided radiotherapy uses advanced imaging technology to localize the target volume, minimizing spatial uncertainties associated with treatment. (Xing et al., 2006). Cone-beam CT mounted on the linear accelerator is used to achieve this objective (Jaffray et al., 1993; Topolnjak, 2005). Prior to treatment delivery, patient CT images are acquired and compared to those of treatment simulation to aid in applying the necessary corrections to the patient set-up. Being able to recognize the site provides high accuracy in treatment delivery with the radiation IGRT is particularly beneficial for the treatment of cancers in parts of the body that are prone to motions, example lungs or for sites near major organs and tissues that should not receive radiation like the heart or kidney.

2.1.4 Volumetric Arc Therapy (VMAT)

New extension of conventional IMRT is called volumetric modulated arc therapy (VMAT). In this an optimized 3D dose distribution may be delivered in a single gantry rotation. Volumetric modulated arc therapy is said to be the predecessor to RapidArc (Topolnjak,2005).

Compared to conventional radiation treatment (VMAT) highly decreases treatment time by using single or multiple beams which rotates round the patient. This new technology also gives the radiation oncology personnel extra control and flexibility to distribute a

cautiously targeted dose so that only the target receives a high dose of radiation. Three-dimensional imaging technology aids in the precision of the radiation, giving the personnel the ability to see the tumor at the time of treatment. This is an approach of delivering tomotherapy treatment with linacs.

2.2 Tomotherapy IMRT

Two researchers, Cormack and Brahme started the technique of IMRT, in the early 1980s (Cormack, 1987; Brahme, 1988). Separately both showed that there is a higher conformity of dose to the target to be treated while sparing the normal tissues from radiation when non-uniform intensities are used. From then, various procedures of IMRT have been studied which tomotherapy is one of them.

Slice therapy is another name for tomotherapy which is attained from tomography. Mackie et.al (1993) proposed tomotherapy as a procedure to give extremely conformed dose deliveries. Tomotherapy has radiation source mounted in a ring gantry as in CT scanners. The source gives a fan beam of radiation, which moves round the patient as the patient is translated through the ring gantry. The intensity of the fan beam is modulated via MLC which is made up of a series of tungsten leaves which can be manipulated separately. Two forms of tomotherapy have been studied. Nomos Corporation developed serial-tomotherapy also called sequential-tomotherapy and was the first to be used in the clinical world, (Mackie, 2006; Carol, 1995). In serial tomotherapy a narrow rotating beam of radiation is used to irradiate two slices at the same time. The modulation of the intensity is done via two sets of binary collimators. As shown in Figure 2:2, the couch is translated in

discrete steps after one whole rotation of the gantry to deliver the next two slices. Serial tomotherapy utilizes MIMiC(R) binary MLC mounted to the linac; which consists of a set of twenty tungsten leaves that modify the fan beam with a highest field size of 2×20 cm^2 at the gantry isocenter. These leaves can also modulate the radiation into 1×2 cm^2 respectively. The modulation of intensity is via moving the leaves in and out of the beam. This technique is often used in the treatment cancer of the head, prostate and neck (Van Dyk, 1999; Mackie, 2006). Serial-tomotherapy type of IMRT is easily affected by indexing and movement of patient for the next slice treatment; because there are fast dose variations in IMRT treatments, small movement can have a great effect on the total dose distribution accuracy.

Figure 2.1- Tomotherapy system (www.medicalphysics.org, 05/12/2018).

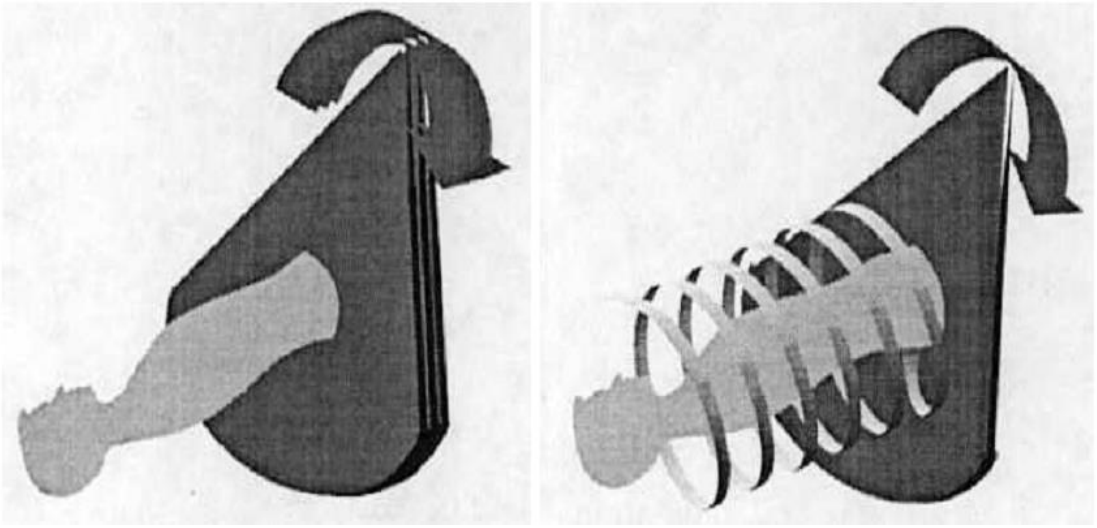

Figure 2. 2- Illustration of serial and helical tomotherapy (Illustration adapted from Van Dyk (1999).

Researchers have proven that the indexing of patient in serial-tomotherapy leads to uncertainties in dose at the junctions of the slices (Low, 1997; Carol et al., 1996); because of these issues with serial tomotherapy T. R. Mackie and the University of Wisconsin research group advanced tomotherapy and called it helical-tomotherapy (Mackie et al., 1993; Mackie, 2006). The system became accessible in the market in the year 2003. In helical tomotherapy, the couch is translated continuously as the radiation moves round the patient continuously as compared to serial – tomotherapy; this decreases the possibility of under dose and over dose at the region that is junction between the slices. The geometric properties of helical-tomotherapy are the same as helical computed tomography scanner. The radiation intensity is modulated by binary miniaturized -MLC. This collimator is made up of 32 pairs of leaves, projecting the fan-beam of up to 40 cm in length (in-plane) and 5 cm in width (cross-plane). Due to the broadness of the fan beam, a larger patient area can

be treated. Also, the beam is modulated to a length of 0.625 cm by each leaf; this makes that type of tomotherapy to deliver better modulated radiation. Helical tomotherapy machines are combined with megavoltage CT for treatment verification, localization and image guidance. Linear accelerators are used as X-ray radiation source for serial and helical tomotherapy method due to this both approaches are mechanically complex. The Cancer Centre of Southeastern Ontario and Queen's University medical physics research group and L. J. Schreiner proposed Co-60 based tomotherapy approach (Schreiner et al., 2006; Gallant et al.,1998). From Schreiner et al., Co-60 based radiotherapy has become inferior because of the absence of improvement. From their work they showed that the large penumbra and beam penetration problems with the Co-60 units can be reduced through tomotherapy for dose delivery. In terms of safety, power supply, maintenance and cost the Co-60 tomotherapy is superior to linacs

Pencil beam radiation measuring 1×1 cm at the isocenter of Co-60 unit was the first to be used for Co-60 tomotherapy. The gantry of the Co-60 unit (Theratron 780C, Kanata, Ontario) was immobile and the phantom was translated and revolved round the isocentre using a mechanized rotation-translation bench top apparatus to mimic a 2-D tomotherapy delivery. The intensity of the beam was regulated depending on the time the beam was permitted to stay at a location. Entirely; the performance of the scanned pencil beam looked like a modulated fan beam from a multi-leaf collimator (Kerr et al., 2000). Initially outcomes got by simple forward planning procedures proved clinically applicable and agreement between the simple tomotherapy plans and their deliveries (Salomon's et al., 2003).

2.3 DOSE VERIFICATION METHODS

Conformal radiotherapy treatment plans can be obtained through the help of refined computer usage. Clinically the plans cannot be used unless the planned dose distributions are proven. Preferably it is better to prove the treatment plan through a true in vivo test. Hence, a specific dosimetric verification process is needed. Indirectly one approach to validate the dose is to expose a phantom and equate the total dose distribution in the phantom to the distribution planned by the treatment planning system for that phantom (Nelms and Jursinic, 2003). The differences between measured and calculated doses is attained by superimposing calculated and measured dose contours. This procedure is appropriate when both the plan and the delivery show good agreement (Schreiner, 2006). The dose difference between the measured and calculated dose called dose difference maps can also be used. These maps are very subtle to minor spatial shifts owing to mistakes in the treatment setup or calculations (Mah et al., 1989). At the steep dose gradient slight shifts leads to high dose difference between the measured and the calculated (Harms et al., 1998). The distance-to agreement (DTA) map which provides the distance between a measured data point and the closest point in the calculated dose distribution, can consider these minor shifts and gives a better comparison of dose in high dose gradient areas than dose difference maps (Shiu et al., 1992; Harms et al., 1998).

Nevertheless, the difficulty of the procedure is that it displays great differences in the shallow dose gradient areas even if the dose difference is very minor (Low and Dempsey, 2003). Since steep dose gradient areas are lesser in size than shallow dose gradient areas, many DTA distributions show areas of deviation greater than the one that is clinically standard. Harms et al. (1998) recommended that these two techniques should be used

together rather than individually to relate both low doses gradient and high dose gradient areas. Low et al. used this method to develop a gamma dose distribution method (Low and Dempsey, 2003; Depuydt et al., 2002). The gamma dose distribution procedure, based on the dose and distance criteria (typically in agreement within 3% in dose and 3 mm in distance is required), assigns a value of 1 or less to the areas where there is a good agreement between two distributions and a value higher than 1 where the agreement fails (Low and Dempsey, 2003; Depuydt et al., 2002).

The choice of dose measurement tools is a significant part of the dosimetric verification. There are some various mechanisms that can be used for dose measurements. Ionization chambers, thermoluminescent dosimeters (TLDs) and diodes are clinically used for point measurements for 1-D system. 1-D systems are not adequate for IMRT since it is not feasible to validate an IMRT plan point by point. In IMRT dose drop off is usually high at small spatial displacement usually at the edge of the target and is non-uniform in the target volume (Schreiner, 2006; Ezzell et al.,2003). To correctly prove 2-D IMRT plan, the data needs to be sampled with a good spatial resolution over some measurement volume, multiple arrays of detectors and films are used for 2-D dose verification techniques

2.3.1 One-dimensional dose verification system

In radiotherapy clinics ionization chambers are usually the instrument for point radiation dose measurements (Duggan and Coffey, 1998). They are made of a volume of gas filled enclosed between two conducting electrodes (Podgorsak, 2005). After Voltage is applied between the electrodes ion pairs are created the cations are attracted to the cathode and

anions to the anode. This generates ionization current which is measured by electrometer. Ionization chambers are placed within a tissue equivalence phantom in dose verification and absorbed dose is measured.

Advantages of ionization chamber are; high precision, direct readout long-term stability, and easy to use (Duggan and Coffey, 1998). The spatial resolution of ionization chambers is not enough due to their big size and this is the major disadvantage of them because it leads to dose discrepancies due to volume averaging.

In clinical radiotherapy centers TLDs are also commonly used for dose verification and detection (Duggan and Coffey, 1998). Thermoluminescence dosimeters are crystalized material containing a phosphor, such as lithium fluoride or calcium fluoride (Khan, 1984). When exposed to radiation, TLD absorbs energy and this causes the electrons in the crystal to move to excited state and the electrons stays in the excited state due to the impurities in the crystal unless heated. When heated, these excited electrons fall back to their ground orbital state with the emission of photon whose energy is equal to the energy difference between the excited state and ground state. Photomultiplier tube is used to count the number of photons and is proportional to the dose received by the crystal. Some factors that can affect TLDs response are the gas surrounding them during readout, the time and nature of storage between exposure and readout their past thermal and radiation history, (Duggan and Coffey, 1998).

Smaller sizes, tissue equivalence, field size dependence usually negligible are the chief advantages of TLDs. The main disadvantage of TLDs is their relatively poor

reproducibility, usually 2%, even when calibration is done cautiously with good equipment (Duggan and Coffey, 1998)

The sensitivity of diodes is normally higher than ionization chambers (Duggan and Coffey, 1998). For this reason, they are suitable for determining steep dose gradients in areas such as the penumbra. Semiconductor diode is made from silicon-based p-n junctions where the depletion zone is generally free of charge carriers (Van Dyk, 1999). When the diode is irradiated the charge, particles are set free and there is current flow. The current measured is equal to the energy absorbed by the detector. The linearity, reproducibility and stability, of the diode's dose response are good. Some of the shortcomings of semiconductor diodes are; higher atomic number of silicon that is 14. This leads to higher energy dependence compared to ionization chambers (Duggan and Coffey, 1998). They show radiation damage and hence, require re-calibration as their radiation sensitivity decreases with increasing radiation. Owing to their assembly they also exhibit direction dependency, which has major effects in various instances. The three forms above deliver point measurements only and are not used for 2-D IMRT dose verification. 2-D array of diodes and ionization chamber can be used for IMRT verification.

2.3.2 Two-dimensional dose verification system

Measurement of radiation doses to high precision in a 2-D plane can be measured with several dosimeters. The 2-D array of detectors offer fast technique for day-to-day IMRT dose verification and QA. They vary a little depending on the number and type of the detectors, their dimensions and how they are arranged with respect to the beam. A study was done by Amerio et al. (2004) and Herzen et al. (2007) on ionization chamber Matrix which contained 1024 chambers arranged in a matrix of 32 x 32 chambers,5 mm height , 4.5 mm diameter and center to center chamber spacing was 7.62 mm. They recorded excellent signal linearity with respect to dose-rate and dose. Moreover, their outcome produced a very good reproducibility with values remaining within 0.5 % over one month of daily measurements. Poppe et al. (2006) did a study on two other types of 2-D arrays of chambers to find their potential for IMRT verification. These two detectors were Version 1 (256 ionization chambers in a 16 x 16 matrix) and Version 2 (729 ionization chambers in a 27 x 27 matrix) of 2D-array (PTW-Freiburg, Germany). They showed an excellent short-time reproducibility of 0.2% and long-term reproducibility within 1% over a period of 4 months.

Even though the 2-D array of detectors give fast way for dose verification, their spatial resolution is very limited. Hence for a good spatial resolution film is a better choice for verification of plans. Radiochromic and radiographic are the types of films are mostly used. The radiographic film comprises of a radiation sensitive emulsion coated on a transparent polyester base (Khan, 1984). The emulsion is made up of silver halide crystals imbedded in gelatin. When exposed to radiation, excitation and ionization occur in the silver halide

which results in latent image formation. After the development of the film, the affected crystals are reduced to small grains of metallic silver, making it opaque.

Radiographic film application in linac based IMRT and tomotherapy dose verification has been evaluated widely (Oldham and Webb, 1997). The main disadvantage of this type of film is that its response to dose is easily affected by variables like chemical processing (Khan, 1984). Minor changes in processing conditions can greatly influence the dose response. Hence, to avoid discrepancies emanating from processing conditions, another film-based dosimeter, radiochromic film, has been developed. It has the integrating and geometric benefits of radiographic film. It does not need chemical processing (McLaughlin et al., 1996).

Radiochromic reactions are direct coloring of a medium by radiation absorption, without needing any latent thermal, chemical or optical development. It works equally as radiographic film it is made up of a radiation-sensitive monomer when radiated and the film automatically darkens. In spite of its self-developing characteristic which has significantly reduced the verification process; its application in clinics are limited

CHAPTER THREE

3.0 INTRODUCTION

This chapter outlines the materials and methods used for the research work. The design and fabrication of turn table and the procedures used to conduct the research work are also discussed.

3.1 Materials

The materials used in this research involves Co-60 teletherapy unit (Cirus Cobalt-60, France), plastic phantom (PTW, Freiburg, Germany), Farmer type ionization chamber (PTW, Freiburg, Germany), UNIDOS, Electrometer (PTW, Freiburg, Germany), Turn table.

3.1.1 TURN TABLE FABRICATION

The steel metal of 19 feet and mass of 1.4kg was initially cut to make a block by using a glass cutter; this was done to make the metal nicer and smoother. The metal block was then sent to the lathe machine to make the block smoother and brighter so that the turn table shape will be made perfectly. The constructed turn table of total weight 38kg consists of one speed wiper motors of 22 revolution per minute(rpm) connected to a metal thread and two speed wiper motor of 35rpm(low) and 50rpm(high) connected to two transformers to control the translation and rotation of the phantom; the motion of rotation and translation is controlled by a switch. When irradiating, the gantry of the Co-60 unit remains stationary

at 90^0producing a horizontal beam. The phantom rotates and translates in front of the beam, mimicking an intensity modulated fan beam like tomotherapy.

Figure 3. 1 -Lathe machine used for the fabrication of turn table

Figure 3. 2 - Initial stage of turn table

Figure 3. 3-Final stage of turn table

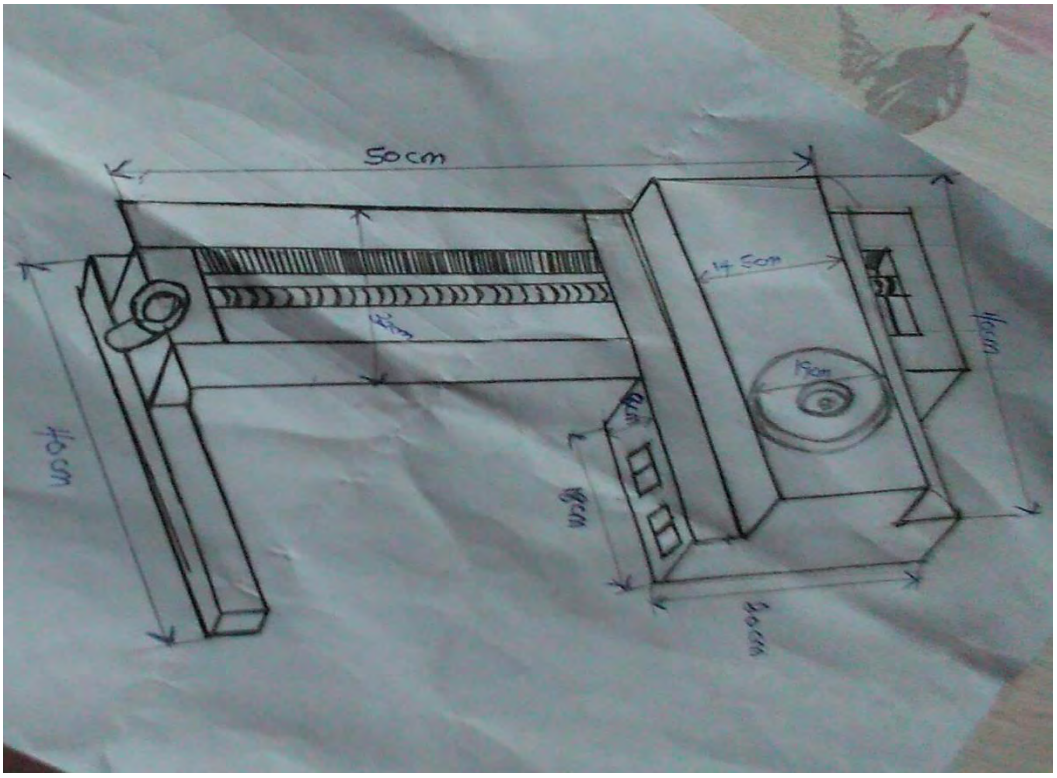

Figure 3.4 - Technical drawing of the Turntable

3.1.2 The Farmer Type Ionization Chamber

The field ionization chamber used in this work was a Farmer type manufactured by PTW Freiburg with model number W-30010 and serial number 129 (Figure 3.4). It was used with the water equivalent phantoms to determine the doses delivered to the various organs. It has a sensitive air volume of 0.125 cm^3 that is open to the environment and therefore, its readings need to be corrected for factors like temperature, humidity and pressure that affect air density. Its calibration was done by the method of substitution using the IAEA reference standard chamber NE-2561/NPL (#321). The calibration coefficients were established at the conditions 20.0^{0}C temperature, 101.325 kPa pressure and 50.0% relative humidity.

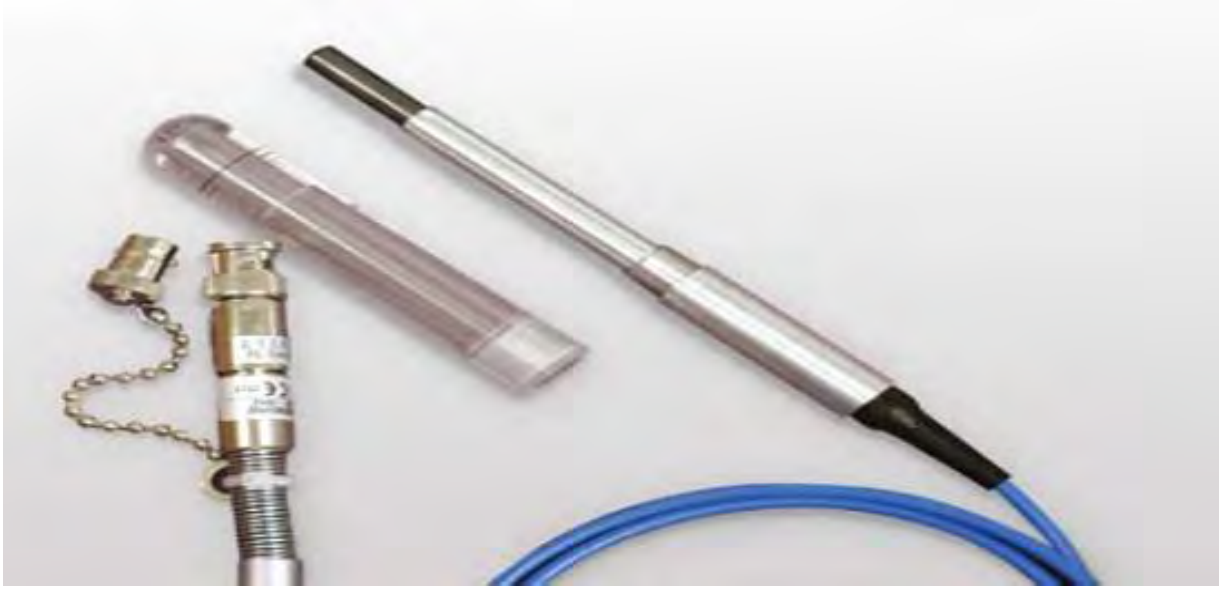

Figure 3. 5- Thimble Farmer Chamber

3.1.3 Co-60 Radiotherapy Unit

Cirus Cobalt-60 teletherapy machine is an isocentric teletherapy cobalt unit. The system combines the following features, minimum field size of 4 cm x 4 cm, availability of collimator, couch, gantry, upper and lower symmetric jaws, weight capacity of couch 130 kg and reference distance set up of 80 cm source-to-skin distance (SSD). The machine is licensed to hold cobalt-60 (^{60}Co) radionuclide with 2 cm diameter confined in a stainless steel shell filled with natural uranium and lead. It is made to load cobalt-60 source of maximum activity of 228.0 TBq (10785 Ci). Figure 3.5 shows the cobalt- 60 teletherapy machine in use at the Oncology Directorate of the Komfo Anokye Teaching Hospital (KATH). The two (2) jaws of the collimator are symmetric and move together in X, Y directions from zero position to the maximum opening. The maximum symmetrical field size achievable is 32 cm x 32 cm at 80 cm SSD.

Figure 3. 6-Cobalt- 60 teletherapy machine in use at the Kath Oncology Department

3.1.4 Electrometer

The electrometer used was PTW UNIDOS model with serial number T10005-50316. It was calibrated together with the ion chamber used for this study. The electrometer was used to quantify charges that had been collected by the ionization chamber in nC/minute. The measured values were then corrected for temperature and pressure variations.

Figure 3. 7- PTW UNIDOS Electrometer

Other Materials

Barometer, thermometer and a solid water phantom of dimension dimensions 30 cm by 30 cm were used for the setup.

Figure 3. 8- Barometer

Figure 3. 9-Thermometer

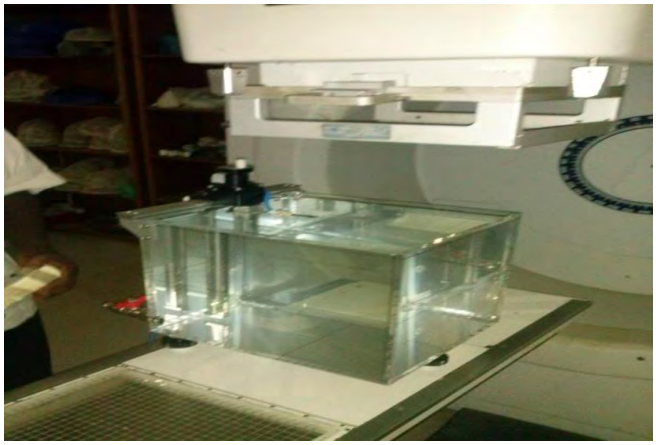

Figure 3. 10- Solid water phantom

1.2 EXPERIMENTAL PEOCEDURE

3.2.1 QUALITY CONTROL/QUALITY ASSURANCE

Quality control tests were performed on the Co-60 treatment unit before clinical measurement was done. This is called absolute dosimetry which consist of absolute dose to water, reference check source and time error measurements. These tests were performed on all equipment before any measurement was taken, and all the equipment were allowed to acclimatize to the room's conditions.

The chamber was pre-irradiated for 5mins to remove traces of stray charges and for stability check. Using a reference standard method comprising of a thimble Farmer type ionization chamber placed at a depth of 5cm within the solid water phantom and connected to an electrometer reading were recorded when the chamber was irradiated by the 60Co source.

The measurement was done as shown in Figure 3.10 at reference setup where the beam central axis of a standard field size of 10cm x 10cm coincided with that on the solid water phantom at SSD of 80 cm to account for recombination, four successive electrometer readings were taken for polarities of -400, +400V, -200V, +200V and 100V by setting an electrometer time of 60 seconds for each voltage.

Figure 3. 11 - Practical setup of the QC measurement with solid water phantom

3.2.2 DOSIMETRY MEASUREMENT WITH THE FABRICATED TURNTABLE

3.2.2.1 Output factor measurement (OF)

Output of the Cirus^{60}Co machine is the dose monitored using a calibrated ion chamber in the head of Cirus^{60}Co machine and calibrated to give 1cGy/mu at 80 SSD and for 10x10 cm^2.Output factor as defined by khan (1984) is also known as collimator scatter factor (Sc**)** which is the ratio of output in air for a given field to that for a 10x10 cm^2 field this is measured by a calibrated ion chamber .In this work a simple translation-rotation turntable, together with a conventional Cirus Cobalt-60 radiotherapy machine was used as a tomotherapy dose delivery system. As illustrated in Figure 3.12. the output factor was found by filling 30x30cm^2 water phantom with water to a depth of 15cm anteriorly and positioned on the turn table on the couch. Farmer type ion chamber secured on retort stand was connected to a PTW UNIDOS electrometer at depth of 0.5cm (D_{max} of cobalt) laterally.

For an open field at SSD of 80cm, field sizes of 4x4cm^2 to 30 x30cm^2 . The Co-60 unit is directed towards the water phantom at an angle of 90 degrees and irradiated a for 60s. While the Co-60 beam remains stationary during irradiation, the water phantom undergoes rotational motion which mimics the irradiation of a single slice achieved with serial-tomotherapy. Charges were collected by the ion chamber and measured using the electrometer; three successive readings were taken for each field size and the average value determined and recorded.

The initial and final temperatures and pressures were recorded using the thermometer and barometer respectively.

The output factor (OF) was then calculated using the formula below.

$$OF = \frac{\text{corrected reading at depth 0.5cm for a particlar field size}}{\text{corrected reading at depth of 0.5cm for 10x10cm(reference field size)}} \quad \text{....(3.1)}$$

3.2.2.2 MEASUREMENT OF TISSUE AIR RATIO (TAR)

Tissue air ratio (TAR) is the ratio of the dose at depth d (D_d) in a tissue to the dose at the same depth in air (D_{air})

$$TAR = \frac{\text{dose at a particular depth(Dd)}}{\text{dose at the same depth in air Dair}} \quad \text{.....(3.2)}$$

The following procedures were used in the determination of TAR

The 30x30cm^2 water phantom was filled with water to depth of 15cm anteriorly and placed on the turn table on the couch

Farmer type chamber of 0.125 cm^3 measuring volume connected to a PTW UNIDOS electrometer was placed at depth of 5cm laterally

For an open field at SSD of 80cm and field size of 4x4cm^2 to 30x30cm^2 at an angle of 90^0 were used to irradiate for 60s at central axis depth of 5cm,10cm 15cm and 20cm

respectively whiles the phantom rotates in front of the beam by turning on the turn table at low speed to mimic tomotherapy.

Charges were collected by the ion chamber and measured using the electrometer. Three successive readings were taken for each field sizes and the average values determined and recorded.

The barometer and thermometer were used to determine the initial and final pressure and temperature respectively and the measured values were then corrected for temperature and pressure.

The same procedure was repeated for measurements in air with the water emptied from the phantom

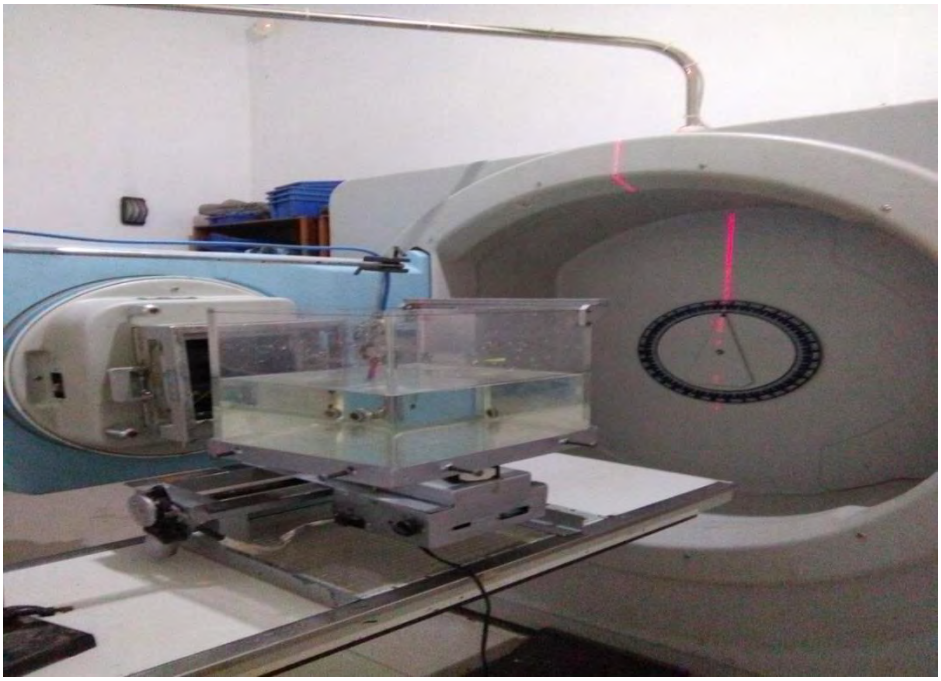

Figure 3. 12- Setup for measurement in tissue

Figure 3. 13- Setup for measurement in air

3.2.3 BEAM PROFILE

In radiotherapy, longitudinal and transverse dose measurements are taken with a radiation detector to characterize the radiation beams from linear accelerators and cobalt-60 teletherapy machines. Photon beams may be represented as a depth dose chart (along the central beam axis), a beam profile (perpendicular to the beam axis), or an isodose chart (a plane parallel or perpendicular to the beam axis). Beam profiles are measured to characterize the dose at points off the central axis, in measuring the beam profile, a 30 x 30 cm^2 water phantom was set up on the turn table on the couch as shown in Figure 3.13. The ion chamber was connected to the electrometer and was attached to the retort stand to hold it in the water whiles the phantom rotates. Charges were collected both in the central axis and off axis as the phantom rotates in the low speed on the couch. For the off-axis

measurement, the chamber was placed 1cm to 5cm away from the central axis both in the positive +x and -x directions. This procedure was done for various field sizes and depths at a constant SSD of 80 cm. At each measurement, three consecutive readings were taken and then averaged. A beam profile was obtained and analyzed.

Figure 3. 14- Setup for beam profile measurement

3.2.4 Pressure and Temperature Correction Factor, PTP

The calibration factors are for standard environmental settings of temperature at to = 22°C and P_o = 110.33 kPa, the readings were corrected by multiplying the average charge by the temperature and pressure correction factors given by the equation:

$$P_{TP} = ((273.2 + T)/ (273.2 + 22.0) \times ((101.33/ P) \quad \ldots\ldots\ldots\ldots\ldots\ldots\ldots\ldots (3.3)$$

Where T is the temperature in degrees Celsius, P is the pressure in kilopascals and PTP is the correction factor. The average readings were then multiplied by the correction factor, PTP to acquire the corrected reading:

$$M_{cor} = M \times P_{TP} \quad \text{(3.4)}$$

3.2.5 DETERMINATION OF DOSE DISTRIBUTION

The dose calculation algorithms that are in standard TPSs can be assigned into two groups, model based and correction-based (Carrasco et. al, 2004). Correction-based systems use correction factors to already measure reference dose distribution data. A simple instance of this approach is the data-driven Milan and Bentley (1974) system. After the correction of temperature and pressure the Milan Bentley formula was used to calculate the dose at point(x,d) as

$$D(x,d) = C(d)R(x,d)\left(\frac{SSD}{SSD+h+d}\right)^2 \quad \text{(3.4)}$$

Figure 3.14 provides the geometry for the pencil beam dose measurement.

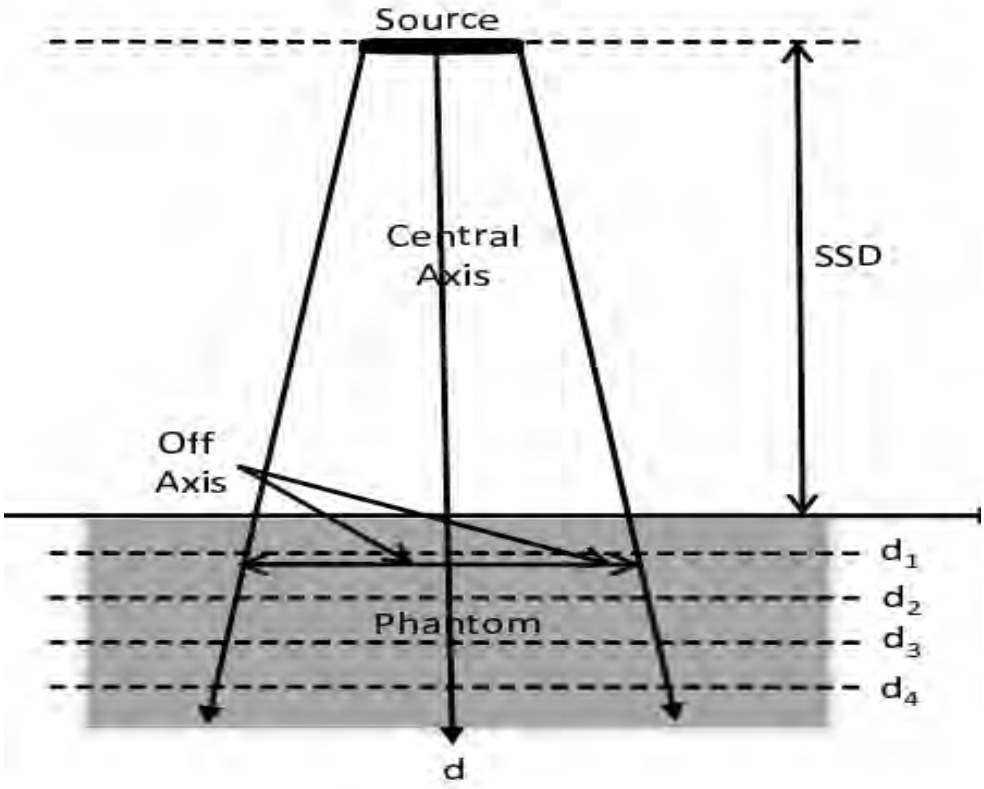

Figure 3. 15- The geometry for the pencil beam dose measurement

Where

$D\,(x, d)$ dose at a point

C(d) is the central axis dose at depth, d and R (x; d) is the off-axis ratio which is given as

$$\left(\frac{\text{Dose at a particular off-axis}}{\text{Dose at the central-axis}}\right) \quad \text{.....(3.5)}$$

Depth, d and off axis distance, x .

Snice the phantom used in this work had a flat surface we assumed the h=0

CHAPTER FOUR

4.0 RESULTS AND DISCUSSION

4.0 INTRODUCTION

The chapter presents and discusses the results obtained from the study. It describes the various results for the quality control, the turn table dosimetry measurements and the various results obtained with graphs. Results for, reference check source measurements, absorbed dose to water determination using TRS 398 protocol, tissue air ratio (TAR) percentage depth dose, beam symmetry ,beam flatness and rotational output factor.

4.2 QUALITY CONTROL MEASUREMENTS

4.2.1 Reference check source measurements

The stability of the chamber is important in precise measurements. A long-lived radionuclide is therefore required to measure and calculate the drift in the ionization stability with time. Table 4.1 shows a typical reading of the stability and constancy of the ionization chamber used for the measurements. PTW Unidos electrometer was used.

Table 4. 1: Reference check source measurements for radiobiological dose (rdgy) 420 examinations using a chamber calibrated in terms of NDW practical data.

No.	Reading [nC]	Time: t [s]	Reading Rate [nC 250s^{-1}]
1	0.677	250	0.002708
2	0.677	250	0.002708
3	0.677	250	0.002708
4	0.677	250	0..002708
5	0.678	250	0.0027120
Mean Q_{mean}	0.6772	**250**	**0.0027088**
Std. dev.	$\left(\frac{Max\ Value - mean}{mean}\right)_{=}$	0.001181	0.0027088

The ambient conditions for the measurements are as follow:

T_{in} [^{0}C]: 23 P_{in} [KPa/mbar]: 97.81 Relative Humidity [%]: 23%

$$K_{in}[T,P]=\left[\frac{273.15+T_C}{293.15}\right]\times\frac{101.3}{B_S}=\frac{273.15+(23)}{293.15}\times\frac{101.3}{(97.81)}=1.0462803$$

T_{fin}[^{0}C]: 24.6 P_{fin} [KPa/mbar]: 97.81 Relative Humidity [%]: 23.4%

$$K_{fin}[T,P]=\left[\frac{273.15+T_C}{293.15}\right]\times\frac{101.3}{B_S}=\frac{273.15+(24.6)}{293.15}\times\frac{101.3}{(97.81)}=1.05193295$$

Where:

K_{in} = Initial correction factor

K_{fin} = Final correction factor

T_{in} = Initial corrected temperature

T_{fin} = Final corrected temperature

P_{in} = Initial corrected pressure

P_{fin} = Final corrected pressure

B_s =Ambient pressure

4.3 Calculation

Measured Check Source value (Q_{meas}) = $Q_{read} \times K[T,P]_{mean}$ = 0.6772 x 1.049106625

= 0.7104550065 nC

Reference Check Source measurement (Q_{quot}) = 0.6984 nC 250 s^{-1} as at

Decay correction factor (f): from 3/12/17 to 01/05/18

Times elapsed = 0.4127 years

Therefore, f = $e^{-\lambda t} = e^{-\frac{0.693t}{T_{1/2}}} = e^{-\frac{0.693\ t}{28.7}}$ =0.99008, $T_{1/2}\ for\ ^{90}Sr = 28.7a$

Deviation, $\Delta = \left(\frac{Q_{meas} - Q_{quot}}{Q_{quot}} \right) \times 100\%$ = (0.7104-0.6984) x 100%

=1.2%

4.4 Absorbed dose to water rate for ^{60}Co teletherapy unit using a chamber

4.4.1 Calibrated in terms of n_{dw} data

Measurements for the absorbed dose to water rate measurements were done for several voltages specifically +400V, +200V, +100V, -100V, -200V and -400V. These yielded results which were in agreements with IAEA protocols

Using the initial temperatures, atmospheric pressures, and the relative humidity,

Table 4.2 Absorbed dose to water rate for Co-60 teletherapy unit using a chamber calibrated in terms of NDW practical data.

No.	+ 400V Reading [nC]	- 400V Reading [nC]	+ 200V Reading [nC]	- 200V Reading [nC]	100 V Reading [nC]
1	1.779	-1.836	1.774	1.835	1.764
2	1.778	-1.836	1.774	1.836	1.766
3	1.779	-1.836	1.774	-1.837	1.766
4	1.779	-1.836	1.774	-1.836	1.766
-5	1.779	-1.836	1.774	-1.836	1.766
6	1.779	-1.836	1.773	-1.837	1.766
7	1.779	-1.836	1.774	-1.836	1.766

8	1.779	-1.836	1.774	-1.836	1.766
9	1.778	-1.836	1.774	-1.836	1.766
10	1.778	-1.836	1.774	1.837	1.766
Mean M_W	1.7787	-1.836	1.7738	1.8362	1.7658

$$K_{in}[T,P]=\left[\frac{273.15+T_C}{293.15}\right]\times\frac{101.3}{B_S}=\frac{273.15+(22.8)}{293.15}\times\frac{101.3}{(97.81)}=1.0455736556$$

Using the final temperatures, atmospheric pressures and relative humidity,

$$K_{fin}[T,P]=\left[\frac{273.15+T_C}{293.15}\right]\times\frac{101.3}{B_S}=\frac{273.15+(23.2)}{293.15}\times\frac{101.3}{(97.82)}=1.0468797998$$

Electrometer calibration factor k_{elec} : 1.00

Polarity correction rdg at +V1: 400 rdg at -V1:400

$$k_{pol}=\frac{|M_+|+|M_-|}{2M}=$$

K_{pol} = 1.7787 + 1.836/ 2 (1.7787) = 3.6147/3.5574 = 1.01610726935

Recombination correction (two-voltage method)

Polarizing voltages: V1 (normal) = +400V V2 (reduced) = 100 V

Readings at each V: M1 = 1.7787 M2 = 1.7658

Voltage ratio V1 / V2 = 400/100 = 4

Ratio of readings M1 / M2 = 1.7787/1.7658 = 1.00730547

$$k_s = \frac{(V_1/V_2)^2 - 1}{(V_1/V_2)^2 - (M_1/M_2)} =$$

$K_s = ((400/100)^2 - 1)/ ((400/100)^2 - (1.7787/1.7658)) = 15/14.992694529$

$= 1.00049055425$

Corrected dosimeter reading at the voltage V1:

$$M = M_1\, k_{TP}\, k_{elec}\, k_{pol}\, k_s =$$

M = 1.7787 x 1.04622672772 x 1.00 x 1.01610726935 x 1.00049055425

= 1.89182546431 nC/min

4.4.2 Calculations

Determination of absorbed dose to water rate ($_5D_{W\ meas}$)

$$_5D_{W\ meas} = M \times K[T,P] \times {}_5N_{DW} =$$

$= 1.89182546431 \times 10^{-9} \times 1.04622672772 \times 2.995 \times 10^{8}$

$Dose\ at\ 5cm = {}_5D_W = 0.584877064$

$$Dose\ at\ 0.5\,cm\,(d_{\max}),\ {}_{0.5}D_W = \frac{{}_5D_W}{0.788} =$$

$$= 0.584877064/0.788 = 0.74222977$$

Reference absorbed dose to water rate at depth of 5cm [${}_5D_W$ (quoted)] = 0.7251 mGy min^{-1} as at

Decay correction factor (f): from 21/01/2016 to 1/05/2018,

Times elapsed =2.444 years

Therefore, f = $e^{-\lambda\ t} = e^{-\frac{0.693\,t}{T_{1/2}}} = e^{-\frac{0.693\ t}{5.269}} = 0.72548,\quad T_{1/2}\ for\ {}^{60}Co = 5.269a$

Deviation, $\Delta = \left(\frac{{}_5D_W\ meas - {}_5D_{W\ quoted}}{{}_5D_{w\ quoted}}\right)\times 100\% =$

= ((0.7422977-0.7251)/ 0.7251) x 100% = 2.36%

Estimated Uncertainty in ${}_5N_{DW}$ of the Working Standard ± 1%

4.4.3 TIMER ERROR

Accounts for differences between timer settings and actual time the beam is ON. It is equal to the negative of the "end effect" or timer error, α. The timer error is most commonly determined using the multiple exposure method:

$$\alpha = t\left((R_n - R_1)\big/(nR_1 - R_n)\right) \qquad \text{.. (4.1)}$$

Multiple exposures, n, of duration t/n are made, and the integrated reading Rn is compared to the reading R1 obtained in a single exposure of duration t.

If α is positive, the irradiation time is longer than the setting on the timer. The timer correction then requires that this time is subtracted; If α is negative, the exposure time is shorter than the timer setting. The correction in this case requires that this time be added.

Table 4. 3 Timer error practical data

Type of Reading	Readings (nC)
R_1	7.104
R_n	7.112

Calculation: $\alpha = t\left({}^{(R_n - R_1)}\big/_{(nR_1 - R_n)}\right)$

$= (7.112) - (7.104)/\ 4(7.104) - 7.112)$

$= {}^{0.008}\big/_{21.304}$

$= 0.0003755163 = 3.755163 \times 10^{-4}$

4.5 TISSUE AIR RATIO DETERMINATION

4.5.1 TAR VARIATION WITH FIELD SIZE

TAR was obtained by using the ratio of the dose at depth d(D_d) in a tissue to the dose at the same depth in air (D_{air}) as shown in equation 4.2 below .TAR depends on energy, depth and field size and since only Co-60 was used energy was not dependent.

$$\text{TAR} = \frac{\text{dose at a particular depth(D}\mathbf{d}\text{) in tissue}}{\text{dose at the same depth in air Dair}} \qquad \ldots\ldots\ldots\ldots\ldots\ldots\ldots\ldots \quad (4.2)$$

The TAR variations with field size and depth were studied. It was found that, TAR increased as field size increased this is due to an increased in scatter which increased the dose and vice versa.as shown in figure 4.1 – 4. 4.

Table 4. 4 Tissues Air Ratio (TAR) obtained with tomotherapy procedure.

Field size/ cm^2	TAR at 5cm	TAR at 10cm	TAR at 15cm	TAR at 20cm
4x4	0.956845	0.931589	0.915735	0.898013
5x5	0.959715	0.932394	0.917589	0.902886
6x6	0.962092	0.932482	0.918221	0.904611
7x7	0.962631	0.934378	0.920302	0.909339
8x8	0.96778	0.936169	0.927716	0.912269
9x9	0.970792	0.937509	0.931492	0.913572
10x10	0.971617	0.93828	0.93343	0.916772
12x12	0.973709	0.9385	0.933791	0.919249
15x15	0.974528	0.941916	0.93661	0.921335
20x20	0.980537	0.94569	0.938716	0.925614
25x25	0.981603	0.946581	0.93894	0.926648
30x30	0.981973	0.948628	0.94274	0.934888

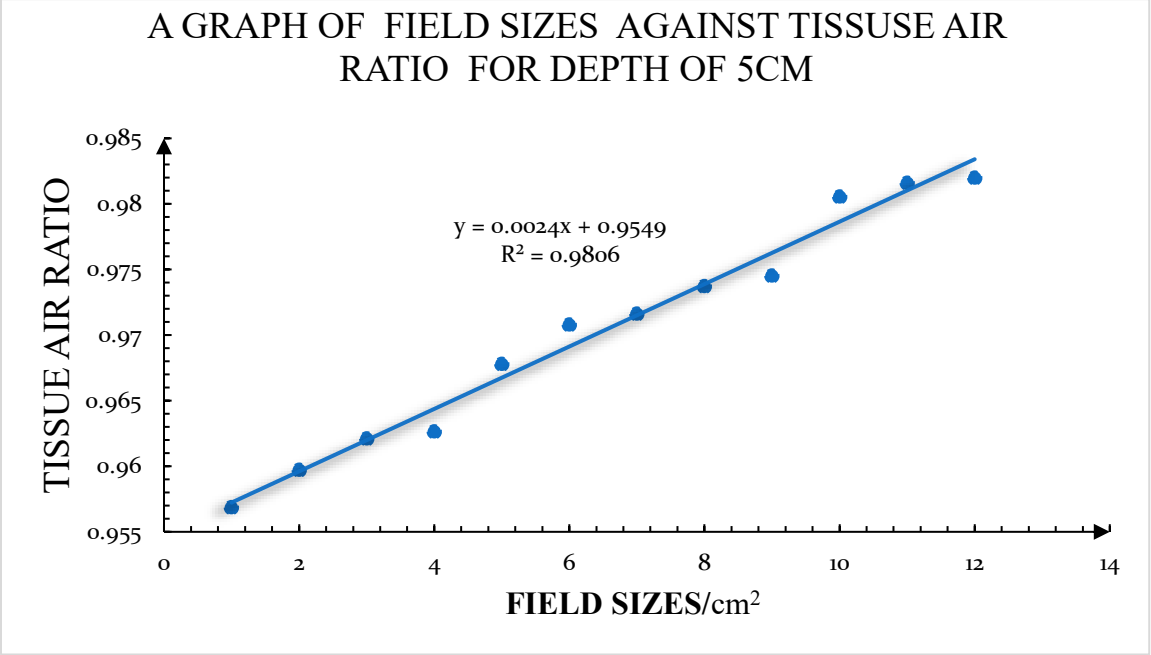

Figure 4. 1- A graph showing variation of field size with TAR at a depth of 5cm

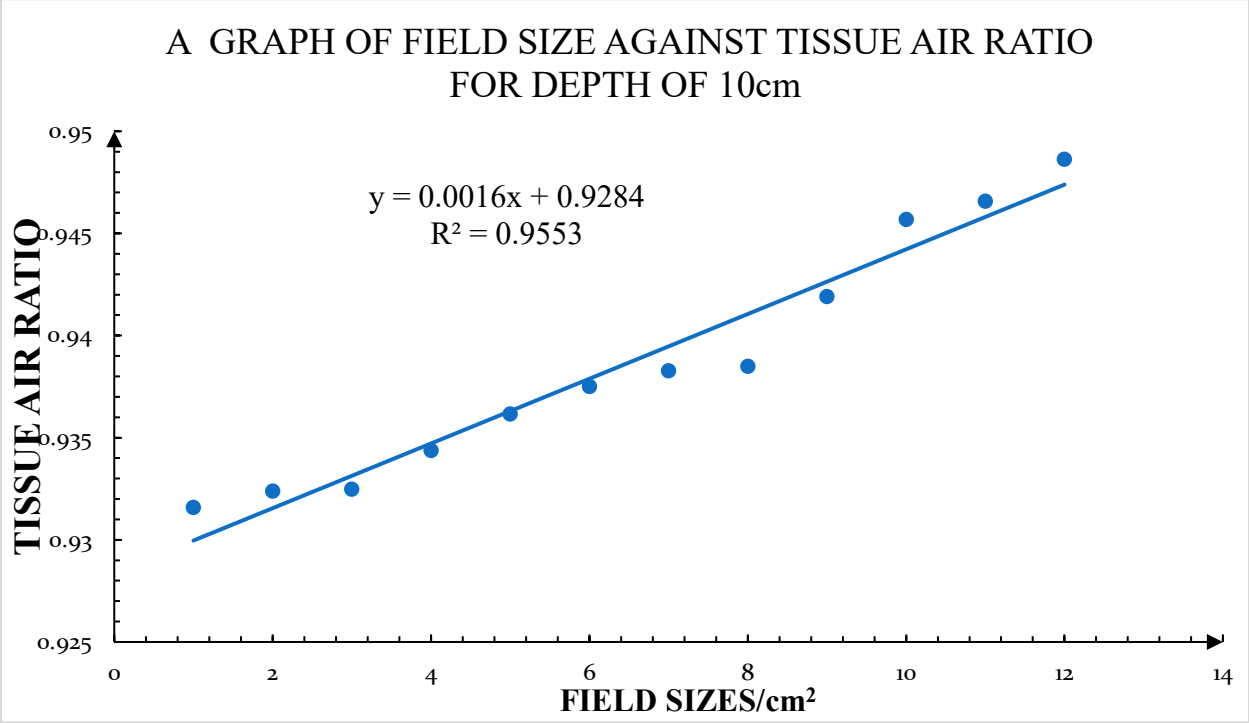

Figure 4. 2- A graph showing variation of field size with TAR at a depth of 10cm

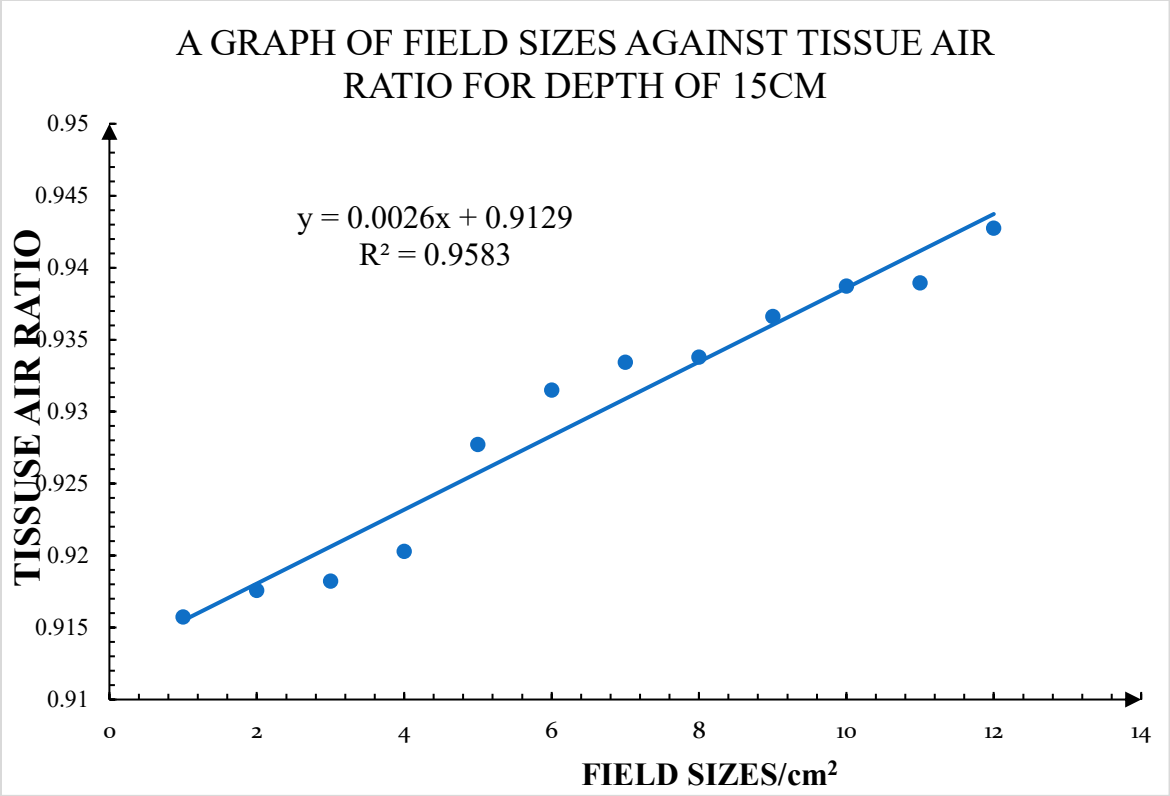

Figure 4. 3- A graph showing variation of field size with TAR at a depth of 15cm

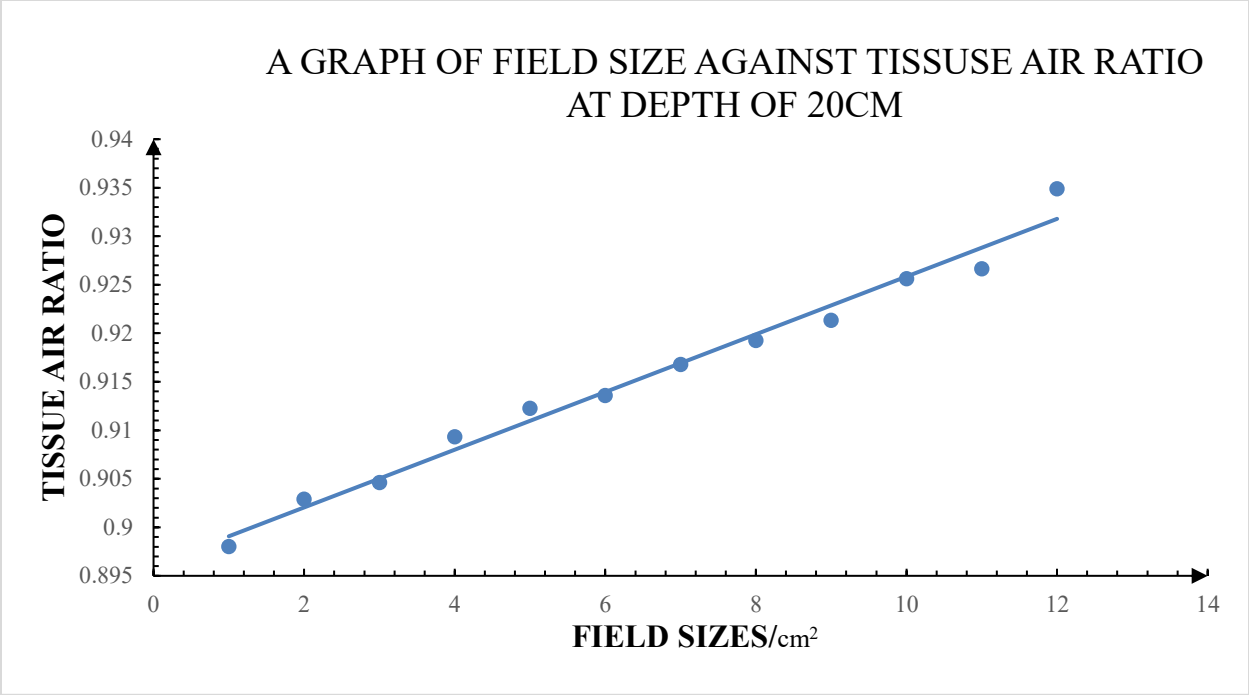

Figure 4. 4- A graph showing variation of field size with TAR at a depth of 20cm

4.6 TAR VARIATION WITH DEPTH

From the results obtained, TAR was found to increase as depth decreased this is due to decreased in dose as depth increases. The graphs below show the variation of TAR with respect to depth

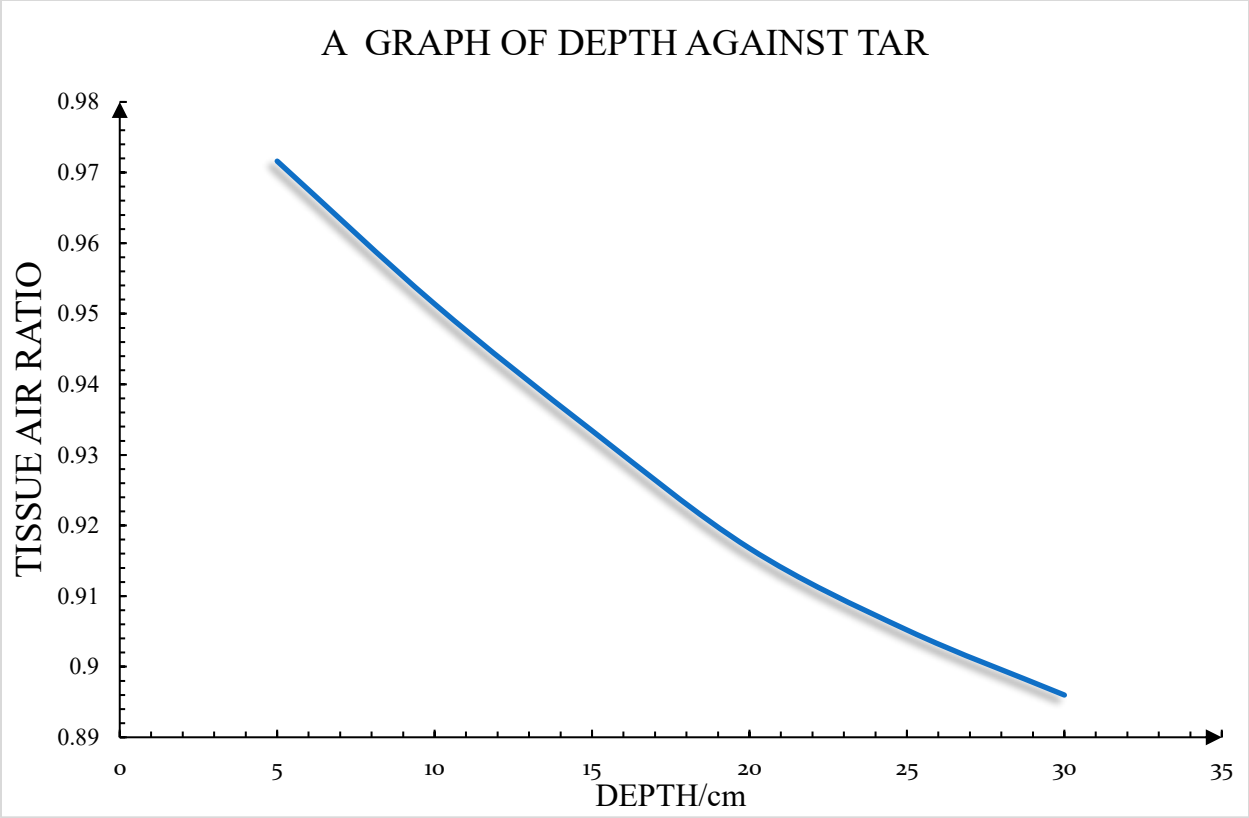

Figure 4. 5- A graph showing depth variation with TAR

4.7 BEAM PROFILE

The accuracy and reliability of each technique in radiotherapy is assessed by analyzing the beam profiles and percentage depth dose (PDD). Beam profile shows the variation of dose occurring on a line perpendicular to the central beam axis at a depth and how doses are altered at points away from the central beam axis.

Beam profile obtained for square field size with varying off-axis depth from 1 cm to 5cm from the central axis depths of 5cm, 10cm,15cm and 20cm in both positive and negative x -direction. From the graphs the maximum dose occurred at the central region (the depth to be treated) and the dose fall of rapidly as the off-axis distance increased. The results for the dose profiles for 10x10, 5x5 and 20x20 field sizes are shown in the figures below (Figures 4.6 and 4.8).

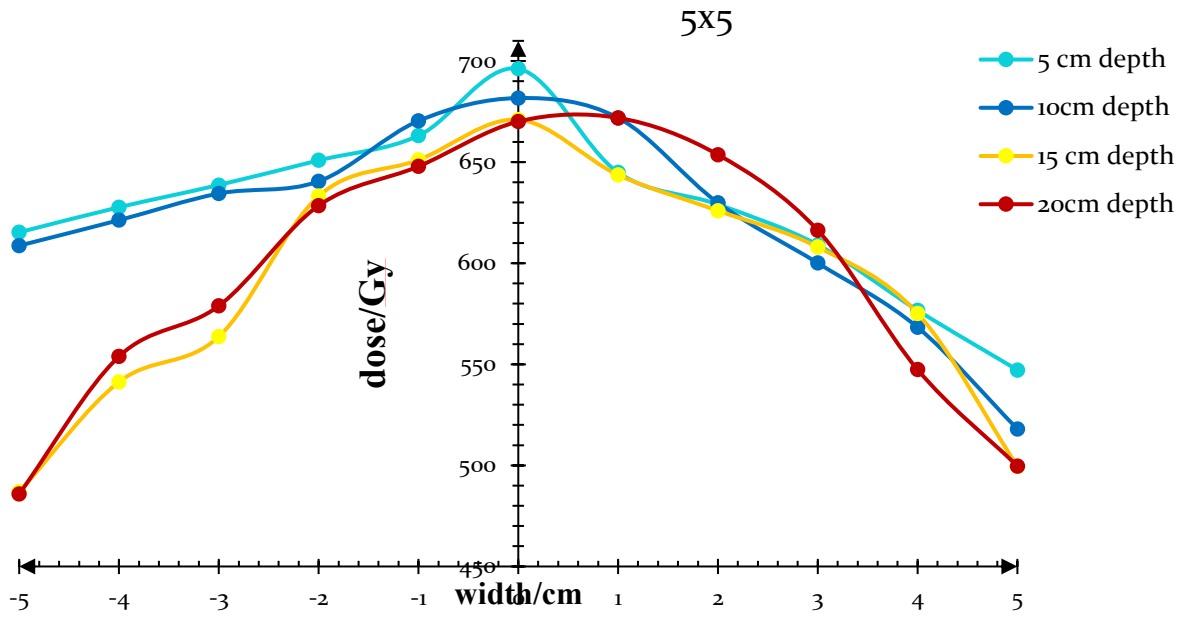

Figure 4. 6- Dose profiles obtained at various depths for a 5x5 field size

.

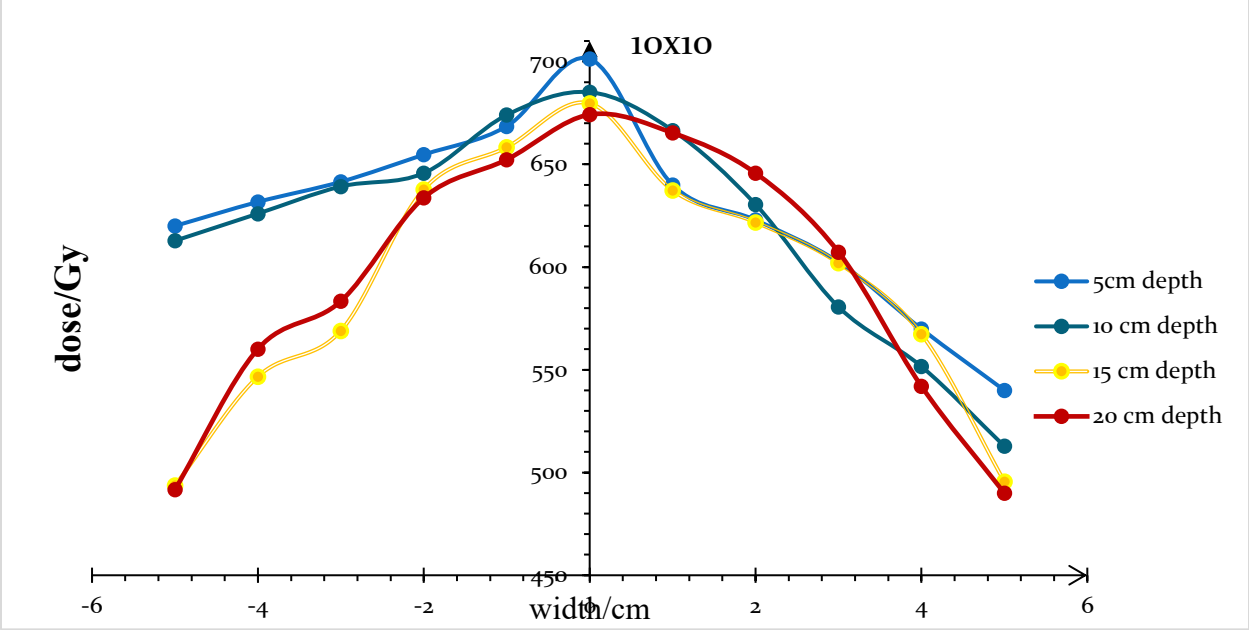

Figure 4. 7- Dose profiles obtained at various depths for a 10x10 field size.

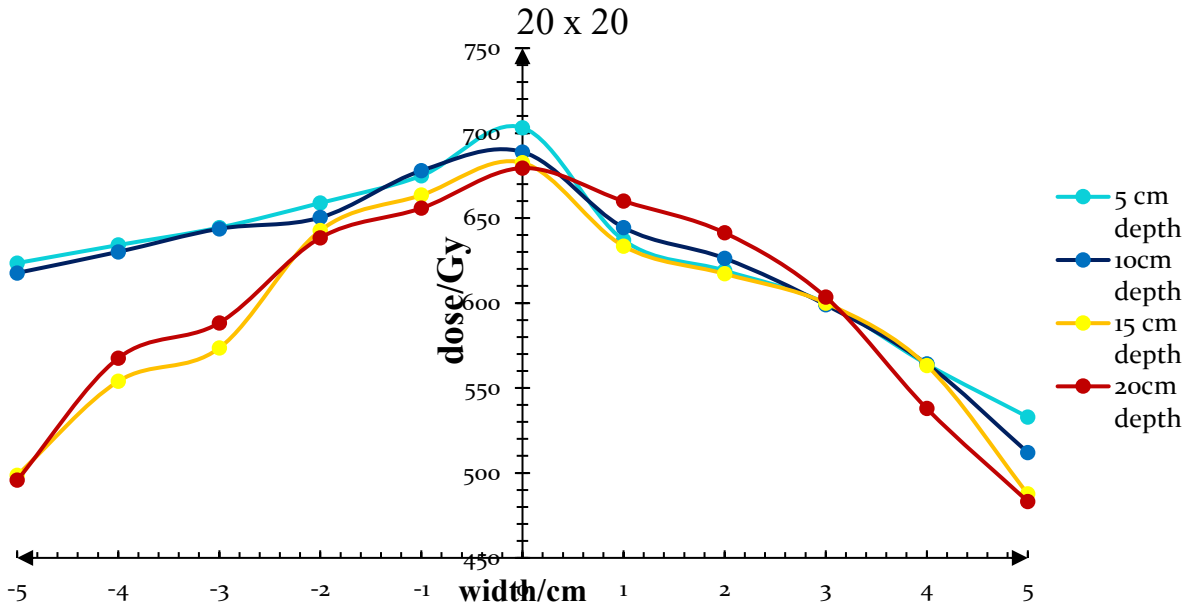

Figure 4. 8 - Dose profiles obtained at various depths for a 20x20 field size

The graphs below also show the effect of field size on the beam profile. From the results obtained, field size was found to increase with dose. At the central axis, the dose was most pronounced at larger field sizes as shown in figures 4. 8 –4. 9.

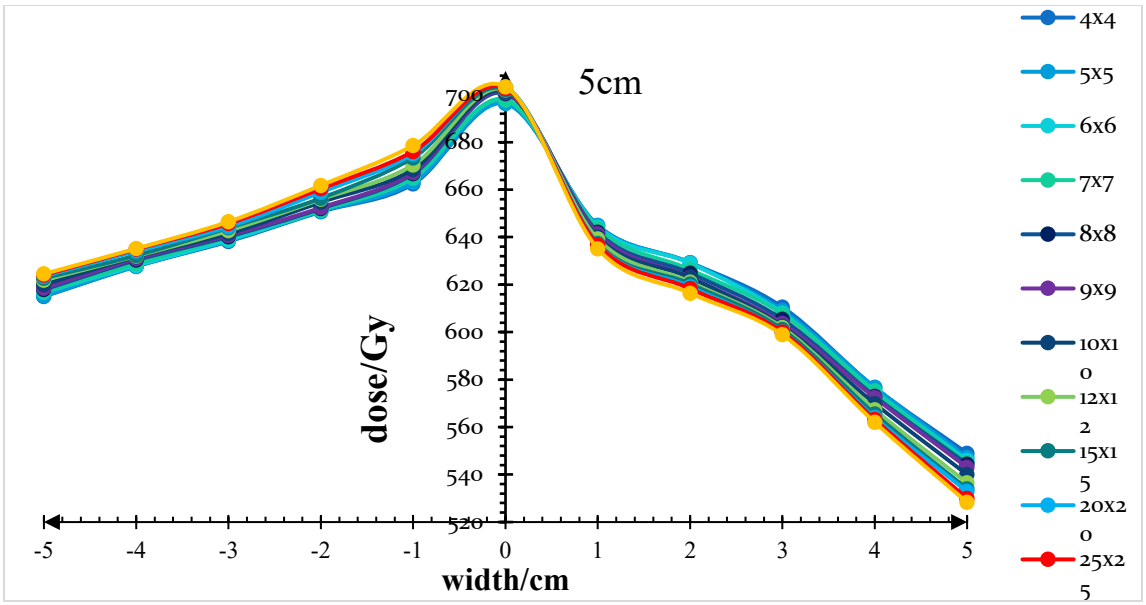

Figure 4. 9 -Dose profiles obtained with constant depth of 5cm and varying field sizes.

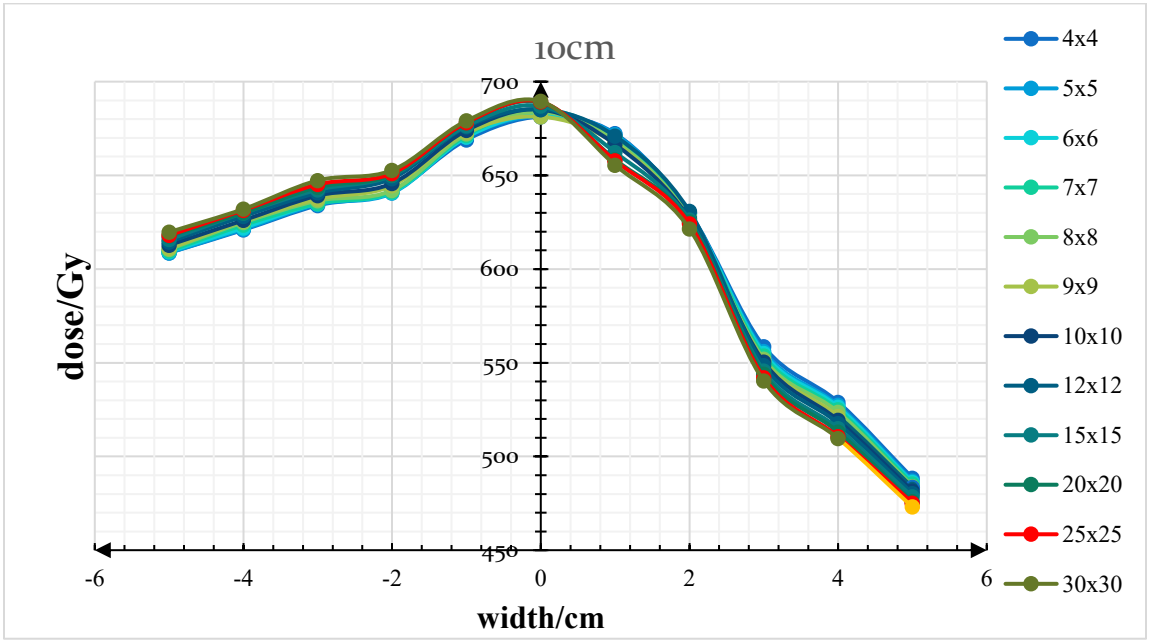

Figure 4. 10 - Dose profiles obtained with constant depth of 10cm and varying field sizes.

4.8 DETERMINATION OF ROTATIONAL OUTPUT FACTOR

Output factors for square field size which ranged from 4 cm x 4 cm to 30 cm x 30 cm were measured at depths of 0.5 cm. The results of the measured data are shown graphically in figure 4.11. From the graph, it can be deducted that the output factors increase with increasing field sizes.

Table 4.5 Rotational output factor of tomotherapy procedure

Field size /cm^2	Rotational output factor
4x4	0.981893
5x5	0.982428
6x6	0.985981
7x7	0.990752
8x8	0.993575
9x9	0.997712
10x10	1
12x12	1.000487
15x15	1.001217
20x20	1.001996
25x25	1.004965
30x30	1.005403

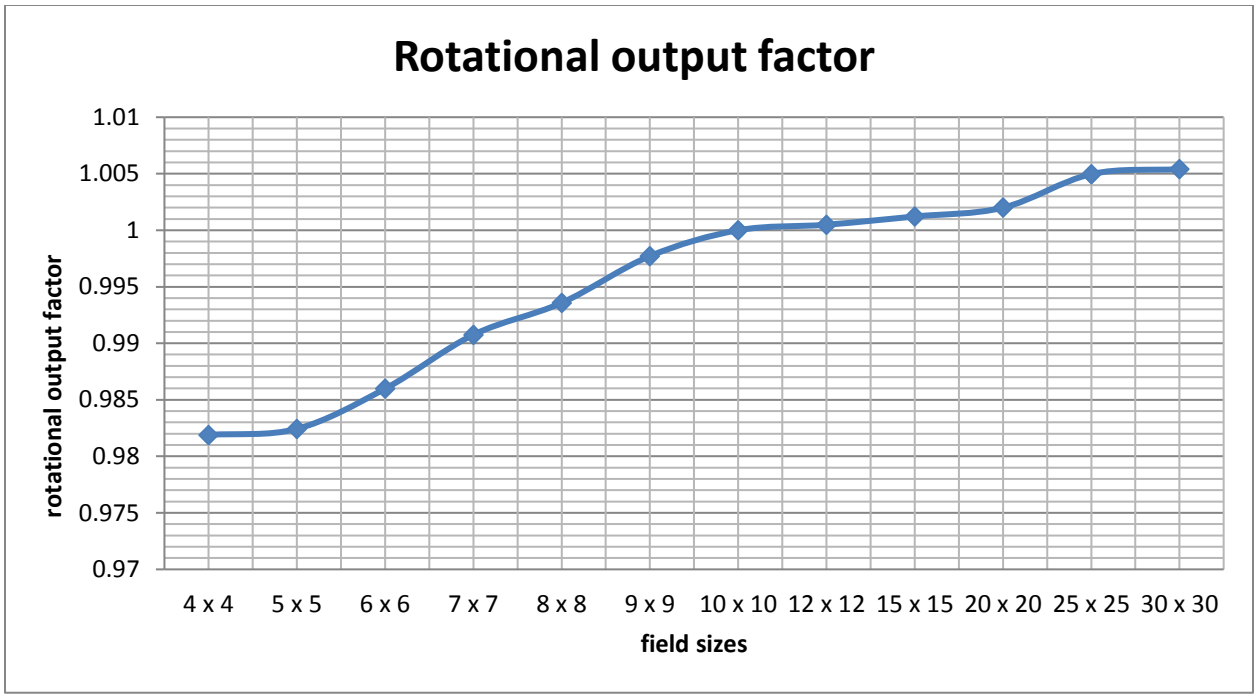

Figure 4. 11- A graph of field sizes verses rotational output factor.

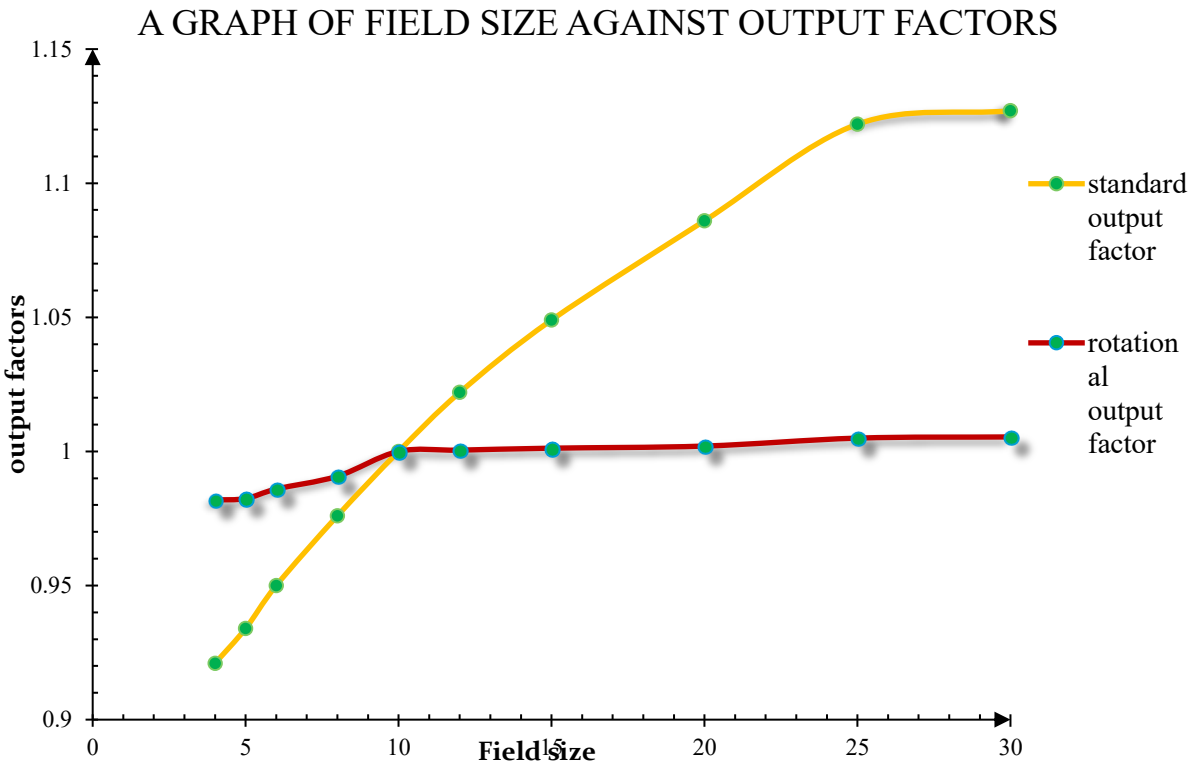

Figure 4. 12- A graph of Field size against output factors

From the graph the graph the rotational output factor and stationery output factor (from the TPS) intersect at the reference field size 10x10cm^2 and the output factors increased as field size increased.

4.9 BEAM FLATNESS (F)

The beam flatness F is measured by finding the and minimum Dmin and maximum D_{max} dose point values on the beam profile within the central 80% of the beam width and then using the formula:

$$\frac{Dmax-Dmin}{Dmax+Dmin}\ x100 = F \quad \text{.....(4.3)}$$

According to the international electro technical commission (IEC) the specification of F should be less than 3% when measurement is done at depth 10cm at SSD of 100cm for the largest field size which is 40x 40cm but in this thesis the largest field is 30x 30cm at SSD of 80cm

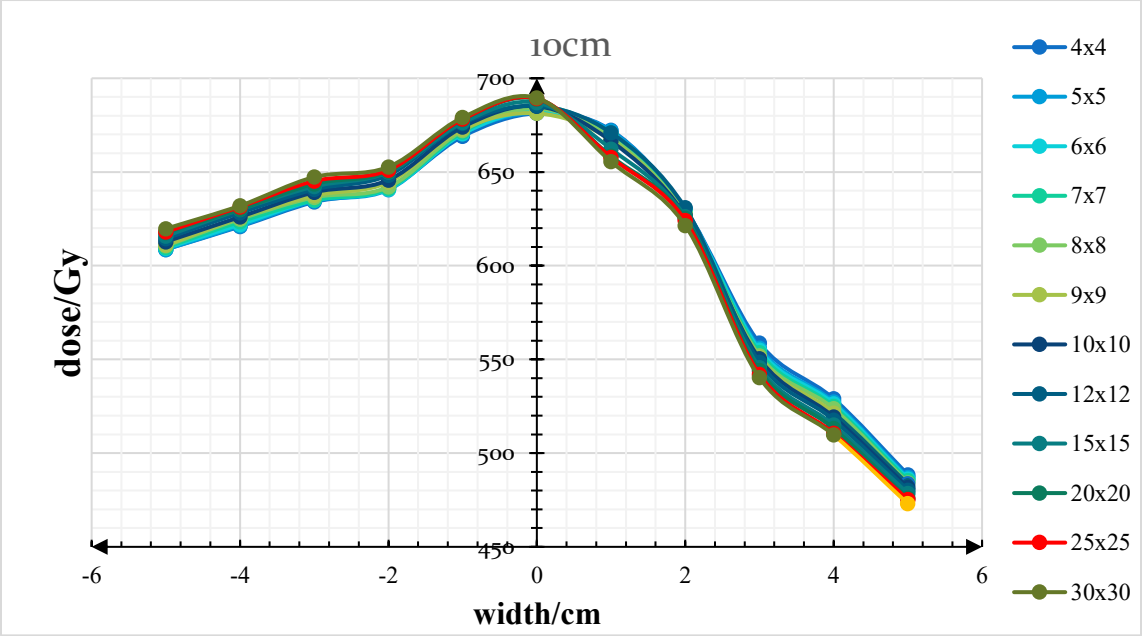

Figure 4. 13- Dose profiles obtained with constant depth of 10 cm and varying field sizes

From the beam profile graph at depth 10cm D_{max}=703.2 and D_{min} =679.4

$$F=\frac{689.5-681.3}{889.5+681.3}\times 100$$

$$F=\frac{8.2}{1371.2}x100$$

F=0.6%

From this it shows that beam profile was flat, and the dose distribution was homogenous

4.9.1 BEAM SYMMETRY(S)

To determine the uniformity between the dose distribution at the x, –x axis beam symmetry is mostly determined and this is measured at an area under Z_{max} on each side i.e. left and right of the central axis .The area under the graph can be determine using either counting square on a graph paper or planimeter .S is calculated using the formula:

$$S=\frac{Area\ left-Area\ right}{Area\ left+Area\ right}x100\%$$ and should be less than 2%..... (4.4)

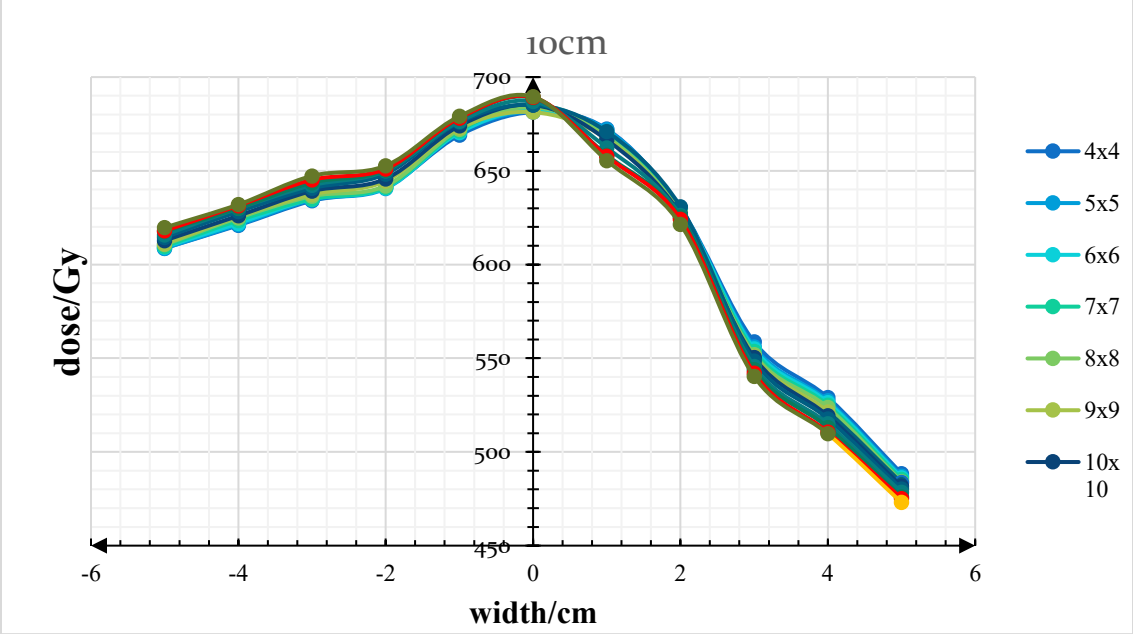

Figure 4. 14- - Dose profiles obtained with constant depth of 10 cm and varying field sizes

At width of 3cm from the central axis using counting square method

Area left =132 and Area right=129

$$S=\frac{132-129}{132+129}\ x\ 100\%$$

S=1.149 %

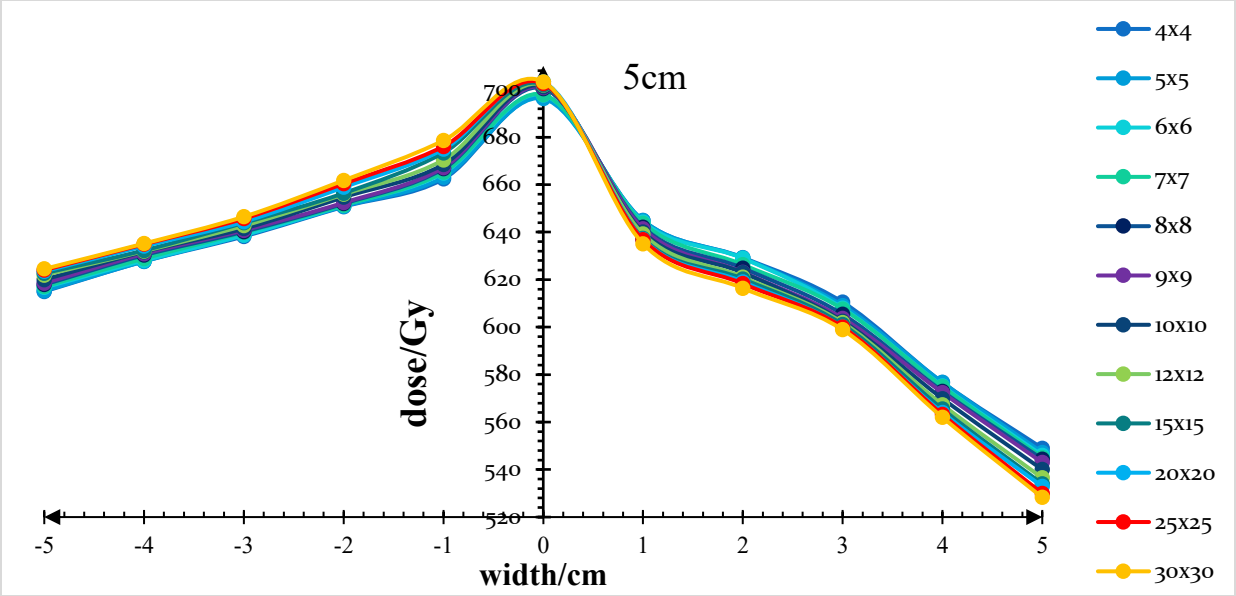

Figure 4. 15- Dose profiles obtained with constant depth of 5cm and varying field sizes.

At width 2cm from the central axis using counting square graph

Area left = 68.5 and Area right = 67.5

$$S = \frac{68.5-67.5}{68.5+67.5} x\ 100$$

= 0.735%

4.10 VARIATION OF PERCENTAGE DEPTH DOSE WITH FIELD SIZE AND DEPTH

Field size (scatter), is proportional to percentage depth dose. The influence of the scattered radiation to the dose absorbed point in the patient increases with respect to field size and therefore the increases in scattered dose happens at larger depths than at depth of maximum dose. Percentage depth dose increases from the surface to a depth of maximum dose which

is 0.5cm for cobalt and then decreases with increasing depth. The variation of PDD as a function of field size and depth is shown in figure 4.16

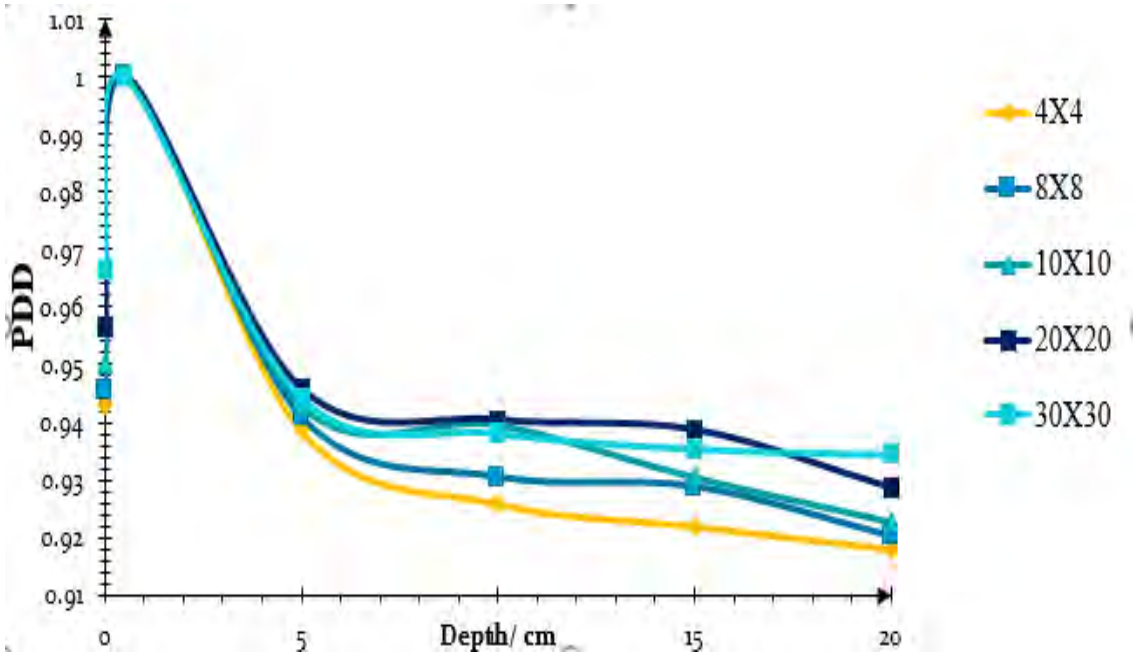

Figure 4. 16- A graph of depth against PDD

CHAPTER FIVE

5.0 CONCLUSION AND RECOMMENDATION.

5.1 Conclusion

The feasibility of emulating tomotherapy treatments with telecobalt machine had been ascertained. Basic beam data and dosimetric functions such as; output factors, tissues air ratios, percentage depth doses, beam profile and beam symmetry to ensure implementation of tomotherapy with a Crius telecobalt machine had been measured and established. The beam flatness and beam symmetry were found to be 0.60 %, and 1.19% (at depth 10cm and width of 3cm from the central axis; and 0.74% at depth 5cm and width of 2 cm from the central axis) which agreed with the International Electrotechnical commission range of 3% and 2% respectively. The output factor increases as the field size also increased due to increase in scatter, the tissues air ratio also increased as depth decreased due to decreased in dose as depth increases. The percentage depth dose increased from the surface to a depth of maximum dose which is 0.5cm for cobalt and decreased as the depth increased. The fabricated turntable shows promising results in the field of to, and reliability of its performance to meet dosimetry and accuracy requirements in the clinical setting.

5.2 RECOMMENDATIONS

Dosimetric parameters should be verify again using the high-speed rotation and compared with the low speed

The turn table design should be improved to be able to regulate the speed of rotation at a time to account for low dose to normal tissue since source strength was equal throughout.

An in-house treatment planning system (primo software) should be used to verify cobalt - 60 tomotherapy on anthropomorphic phantom.

REFERENCES

WHO 2006 Cancer Control: Knowledge into Action-WHO Guide for Effective Programs (Geneva, Switzerland: World Health Organization) (http://www.who.int/cancer/)

Tobias J S 1992 Clinical practice of radiotherapy Lancet. 339, 159-163. [1]

Podgorsak I 2005 Radiation Oncology Physics: A Handbook for Teachers and Students

Van Dyk J 1999 The Modern Technology of Radiation Oncology 1st edn Medical Physics Publishing, Madison Wisconsin. [2, 5, 12, 13, 15, 21, 23, 32, 43, 45, 47]

International Atomic Energy Agency (IAEA), Vienna, Austria. [2, 22, 31, 46]

Schreiner L J 2006 Dosimetry in modern radiation therapy: limitations and needs J.of Phys. Conference Series 56, 1-13. [1, 29, 31]

Foroudi F, Tyldesley S, Barbara L, Huang J and Mackillop W J 2003 Evidence-based estimate of appropriate radiotherapy utilization rate for prostate cancer Int. J. Radiat. Oncol. Biol. Phys. 55,51-63. [1]

Hall E J 2000 Radiobiology for the Radiologist 5th edn J. B. Lippincott Company

Philadelphia. [2]

Ezzell G A, Galvin J M, Low D, Palta J R, Rosen I and Sharpe M B 2003 Guidance document on delivery, treatment planning, and clinical implementation of IMRT: report of the IMRT Subcommittee of the AAPM Radiation Therapy Committee.Med. Phys. 30, 2089-2115. [2, 3, 31]

Purdy J A and Starkschall G 1999 A Practical Guide to 3-D Planning and Conformal Radiation Therapy Advanced Medical Publishing Inc. Madison, WI. [2, 22, 26, 27]

Webb S 2003 The physical basis of IMRT and inverse planning Br. J. Radiol. 76, 678-

89. [3]

Mackie R T 2006 History of Tomotherapy Phys. Med. Biol. 51, R427R453. [11, 12]

Gadza M. J., Coia L.R., Principles of radiation therapy, OncolBiolPhys; 60(1): 365-274, 2004

Williams J.I., Thwaites D.I., Radiotherapy physics in practice, ISBN 0-19-262878-x, 1993.

International Atomic Energy Agency Technical Document (IAEA TECDOC)-1588, 2008

Xing L, Thorndyke B, Schreibmann E, Yang Y, Li Tf, Kim Gy, Luxton G, Koong A, Overview of image-guided radiation therapy, Med Dosim. 31(2): 91-112, 2006.

Jaffray D. A., Battista J.J., Fenster A., Munro P, X-ray sources of medical linear accelerators: focal and extra-focal radiation, Med Phys. 20 (5): 1417-27; 1993

Topolnjak R., The Six-bank multi-leaf system, A large field size, high resolution collimator for advanced radiotherapy, Physics in Medicine and Biology, 50(9): 2015-31, 2005.

Cormack A M 1987 A problem in rotation therapy with x-rays Int. J. Radiat. Oncol. Biol. Phys. 13, 623{630. [11] Cormack A M 1987 A problem in rotation therapy with x-rays Int. J. Radiat. Oncol.Biol. Phys. 13, 623-630. [11]

Brahme A 1988 Optimization of stationary and moving beam radiation therapy techniques Radiother. Oncol. 12, 129-140. [11]

Mackie R T, Holmes T, Swerdloff S, Reckwerdt P, Deasy J O, Yang J, Paliwal B and Kinsella T 1993 Tomotherapy: a new concept for the delivery of dynamic conformal radiotherapy Med. Phys. 20, 1709-1719. [4, 8, 11, 12, 108]

Carol M P 1995 A system for planning and rotational delivery of intensity-modulated fields Int. J. Imag. Syst. Tech 6, 56-61. [11]

Low D A 1997 Abutment region dosimetry for sequential arc IMRT delivery Phys.Med. Biol. 42, 1465-1470. [12]

Carol M, Grant W H, Bleier A R, Kania A A, Targovnik H, Butler E B and Woo

S W 1996 The field-matching problem as it applies to the peacock three-dimensional conformal system for intensity modulation Int. J. Radiat. Oncol. Biol. Phys. 34, 183-187. [12]

Gallant G, Kerr. A, Heath E and Schreiner L J 1998 `A feasibility study of a tomotherapy unit based on Cobalt-60 radiation sources' in `Proceedings of 44th Annual Conference of the Canadian Organization of Medical Physics' London, ON pp. 74-76. [13]

www.medicalphysics.org, 05/12/2017.

Kerr A, Salomons G and Schreiner L J 2000 `Dosimetric Modeling of a Scanned Pencil Beam Apparatus for Evaluation for Cobalt-60 Tomotherapy' in `Proceedings of the 22nd Annual EMBS Internal Conference' Chicago IL pp. 23-28. [14]

Salomons G, Kerr A, Hajdok G, Rogers M, Dyck C and Schreiner L J 2003 `Further Progress in Cobalt-Tomotherapy at KRCC' in `Proceedings of 49th Annual Conference of the Canadian Organization of Medical Physics' Edmonton, AB pp. 40-42. [14]

Jursinic P A and Nelms B E 2003 A 2-D diode array and analysis software for verification of intensity modulated radiation therapy delivery Med. Phys. 30, 870-879.[29]

Mah E, Antolak J, Scrimger J W and Battista J J 1989 Experimental evaluation of a 2D and 3D electron pencil beam algorithm Phys. Med. Biol. 34, 1179{1194. [29]

Harms W B, D. A. Low J W W and Purdy J A 1998 A software tool for the quantitative evaluation of 3D dose calculation algorithms Med. Phys. 25, 1830-1836. [29,

30]

Shiu A S, Tung S, Hogstrom K R, Wong J W, Gerber R L, Harms W B, Purdy J A, TenHaken R K, McShan D L and Fraass B A 1992 Verification data for electron beam dose algorithms Med. Phys. 19, 623-636. [29]

Low D A and Dempsey J F 2003 Evaluation of the gamma dose distribution comparison method Med. Phys. 30, 2455-2464. [30, 34, 58]

Depuydt T, Van-Esch A and Huyskens D P 2002 A quantitative evaluation of IMRT dose distributions: refinement and clinical assessment of the gamma evaluation Radiother. Oncol. 62, 309-319. [30]

Duggan D M and Coffey C W 1998 Small photon field dosimetry for stereotactic radiosurgery Med. Dos. 23(3), 153{159. [31, 32]

Khan F M 1984 The Physics of Radiation Therapy 1st edn Williams & Wilkins Baltimore, MD, U.S.A. [2, 32, 34, 35, 40, 61, 79]

Amerio S, Boriano A, Bourhaleb F, Cirio R, Donetti M, Fidanzio A, Garelli E, Giordanengo S, Madon E, Marchetto F, Nastasi U, Peroni C, Piermattei A, Sanz-Freire C J, Sardo A and Trevisiol E 2004 Dosimetric characterization of a large area pixel-segmented ionization chamber Phys. Med. Biol. 31, 414-420. [33]

Herzen J, Todorovic M, Cremers F, Platz V, Albers D, Bartels A and Schmidt R 2007 Dosimetric evaluation of a 2D pixel ionization chamber for implementation in clinical routine Phys. Med. Biol. 52, 1197-1208. [33]

Poppe B, Blechschmidt A, Djouguela A, Kollho® R, Rubach A, Willborn K and Harder D 2006 Two-dimensional ionization chamber arrays for IMRT plan verification Med. Phys. 4, 1005-1015. [33]

Oldham M and Webb S 1997 Intensity-modulated radiotherapy by means of static tomotherapy: A planning and verification study Med. Phys. 24, 827-836. [34]

McLaughlin W L, Sayeg J A, McCullough E C, Kline R W, Wu A and Maitz A H 1996 The use of radiochromic detector for the determination of stereotactic radiosurgery dose characteristics Med. Phys. 21, 379{388. [35, 36]

Bortfeld T, Boyer A L, Schlegel W, Kahler D L and Waldron T J 1994 Realization and verification of three-dimensional conformal radiotherapy with modulated fields Int. J. Radiat. Oncol. Biol. Phys. 30, 899-908. [3]

Warrington A P and Adams E J 2002 `Cobalt-60 Teletherapy for Cancer - A Revived Treatment Modality for the 21st Century' in `Proceedings of IEE on Appropriate Medical Technology for Developing Countries' London pp. 21.1-21.19. [6, 108]

Schreiner L J, Kerr A, Salomons G, Dyck C and Hajdok G 2003 `The Potential for Image Guided Radiation Therapy with Cobalt-60 Tomotherapy' in R. E Ellis and T. M Peters, eds, `Proceedings of the 6th International Conference on Medical Image Computing and Computer-Assisted Intervention-MICCAI 2003' Vol. 2879. [5, 6, 108]

Low D A, Harms W B, Mutic S and Purdy J A 1998 A technique for the quantitative evaluation of dose distributions Med. Phys. 25, 656{661. [8, 30, 58]

APPENDIX

APPENDIX- I Output factor for square fields of a Cirus Cobalt-60 teletherapy treatment machine using tomotherapy procedure

T1 = 22.5 ºC T2 = 23.8 ºC T average = 23.15 ºC

P1 = 97.84 kPa P2 = 97.79 kPa P average = 97.82kPa P_{TP}=1.04696

Field Size	**Reading [nC] for 60 seconds (1 minute)**					
	1	**2**	**3**	**Mean Q_{mean}**	**Corrected reading= Qmean x P_{TP}**	**Output factor (OF)= $\frac{output(same\ field\ size)}{output\ (10x10)}$**
4 x 4	672.4	671.9	672.9	672.4	703.9756	0.981893
5 x 5	673.1	672.4	672.8	672.7667	704.3595	0.982428
6 x 6	675.5	674.1	676	675.2	706.9071	0.985981
7 x 7	677.7	676.4	681.3	678.4667	710.3272	0.990752
8 x 8	679.4	678.9	682.9	680.4	712.3513	0.993575
9 x 9	684.5	684.4	680.8	683.2333	715.3177	0.997712
10 x 10	684.5	684.9	685	684.8	716.9579	1
12 x 12	685.1	685	685.3	685.1333	717.3069	1.000487
15 x 15	685.6	685.6	685.7	685.6333	717.8304	1.001217
20 x 20	685.8	686	686.7	686.1667	718.3888	1.001996
25 x 25	688.1	688.2	688.3	688.2	720.5176	1.004965
30 x 30	688.4	688.6	688.5	688.5	720.8317	1.005403

APPENDIX -II Absorbed dose to water rate for Co-60 teletherapy unit using a chamber calibrated in terms of NDW practical data.

No.	**+ 400V Reading [nC]**	**- 400V Reading [nC]**	**+ 200V Reading [nC]**	**- 200V Reading [nC]**	**100 V Reading [nC]**
1	1.779	-1.836	1.774	1.835	1.764
2	1.778	-1.836	1.774	1.836	1.766
3	1.779	-1.836	1.774	-1.837	1.766
4	1.779	-1.836	1.774	-1.836	1.766
5	1.779	-1.836	1.774	-1.836	1.766
6	1.779	-1.836	1.773	-1.837	1.766
7	1.779	-1.836	1.774	-1.836	1.766
8	1.779	-1.836	1.774	-1.836	1.766
9	1.778	-1.836	1.774	-1.836	1.766
10	1.778	-1.836	1.774	1.837	1.766
Mean M_W	1.7787	-1.836	1.7738	1.8362	1.7658

Std. dev.	0.0001686625	0	0.0001127523	0.002723015	0.0001132631

APPENDIX III Raw data measurements showing average Ionization Chamber readings in nC for measurements in tissue

T1 = 22.5 ºC T2 = 23.8 ºC T average = 23.15 ºC

P1 = 97.84 kPa P2 = 97.79 kPa P average = 97.82kPa P_{TP}=1.04696

APPENDIX –III.a depth 5cm

field sizes	1	2	3	Average	Corrected readings
4x4	697.9	696	696.7	696.8666667	729.5915253
5x5	698.4	695.3	695	696.2333333	728.9284507
6x6	697.5	698	697.7	697.7333333	730.4988907
7x7	699	696.5	698.1	697.8666667	730.6384853
8x8	700.9	701.6	699.1	700.5333333	733.4303787
9x9	699.6	699.1	703.9	700.8666667	733.7793653
10x10	705.1	699.7	699.1	701.3	734.233048
12x12	698.8	701.7	705.2	701.9	734.861224
15x15	702.5	701.9	701.9	702.1	735.070616
20x20	707	699.8	702.7	703.1666667	736.1873733
25x25	703.2	702.4	702.1	702.5666667	735.5591973
30x30	704.7	702.5	702.8	703.3333333	736.3618667

APPENDIX- III.b Depth of 10cm

field sizes	1	2	3	average	corrected readings
4x4	680.2	680.9	682.9	681.3333333	713.3287467
5x5	683.5	681.9	679.9	681.7666667	713.7824293
6x6	681.6	684.8	681.1	682.5	714.5502
7x7	683.7	687	684.6	685.1	717.272296
8x8	684.8	687.2	679.8	683.9333333	716.0508427
9x9	680.2	680.9	682.9	681.3333333	713.3287467
10x10	683.7	687	684.6	685.1	717.272296
12x12	684.9	684.8	685.8	685.1666667	717.3420933
15x15	689.1	685.9	686	687	719.26152
20x20	691.2	688.3	687.2	688.9	721.250744
25x25	691.1	688.5	688.1	689.2333333	721.5997307
30x30	691.5	689.5	690	689.4888889	721.8672871

APPENDIX –III.c Depth 15cm

field sizes	1	2	3	average	corrected readings
4x4	670.1	669.5	669.8	669.8	701.253808
5x5	670	670	673.1	671.0333333	702.5450587
6x6	671.6	672.3	669.3	671.0666667	702.5799573
7x7	667.3	673.4	676.6	672.4333333	704.0108027

8x8	678	677.3	673.7	676.3333333	708.0939467
9x9	680.6	677.3	677.4	678.4333333	710.2925627
10x10	679.1	682.9	677.2	679.7333333	711.6536107
12x12	676.7	679.1	682.8	679.5333333	711.4442187
15x15	679.3	678.6	685.3	681.0666667	713.0495573
20x20	679.4	684.4	683.9	682.5666667	714.6199973
25x25	682.7	684.3	681	682.6666667	714.7246933
30x30	685.7	684.5	685.9	685.3666667	717.5514853

APPENDIX –III.d Depth 20cm

field sizes	1	2	3	average	corrected readings
4x4	666.1	666	668	666.7	698.008232
5x5	669.9	671.6	669	670.1667	701.6376933
6x6	671.8	669.8	669.3	670.3	701.777288
7x7	671.2	672.8	671.4	671.8	703.347728
8x8	672.9	672.4	672.3	672.5333	704.1154987
9x9	672	673.8	673.4	673.0667	704.6738773
10x10	673.5	674.6	674.5	674.2	705.860432

12x12	671.1	677.5	677.9	675.5	707.22148
15x15	672.4	678.6	678.9	676.6333	708.4080347
20x20	676.8	678.5	683.1	679.4667	711.3744213
25x25	680.3	681.5	677.3	679.7	711.618712
30x30	685.8	681.2	680.4	682.4667	714.5153013

APPENDIX IV Raw data measurements showing average Ionization Chamber readings in nC for measurements in air

T1 = 22.8 ºC T2 = 23.4 ºC T average = 23.4 ºC

P1 = 97.65 kPa P2 = 97.86 kPa P average = 97.76kPa P_{TP}=1.04849

APPENDIX –IV.a READING IN AIR depth 5cm

field sizes	1	2	3	average	corrected readings
4x4	728.9	727.2	725.6	727.2333	762.4968777
5x5	728.5	723	721.7	724.4	759.526156
6x6	723.4	723.4	725.7	724.1667	759.2815083
7x7	721.9	726.4	723.4	723.9	759.001911
8x8	722.5	723.6	722.3	722.8	757.848572
9x9	719.9	719.5	723.3	720.9	755.856441
10x10	722.8	720.1	719.3	720.7333	755.6816927
12x12	722	722	715.4	719.8	754.703102
15x15	719.3	723.2	715.7	719.4	754.283706

20x20	720.8	714.1	711	715.3	749.984897
25x25	710.3	720.7	715.4	715.4667	750.1596453
30x30	716.1	715.7	713.8	715.2	749.880048

APPENDIX IV.b Depth 10cm

field sizes	1	2	3	average	corrected readings
4x4	729	733.9	728	730.3	765.7122
5x5	729.8	730.6	730	730.1333	765.5375
6x6	727	733	728.1	729.3667	764.7337
7x7	729.7	729.9	729.5	729.7	765.0832
8x8	726.8	733.6	728.1	729.5	764.8735
9x9	729.4	730	729.4	729.6	764.9783
10x10	729.9	728.6	728.8	729.1	764.4541
12x12	729.3	730.6	727.1	729	764.3492
15x15	730	726.7	728.2	728.3	763.6153
20x20	727.4	726.9	727.9	727.4	762.6716
25x25	728.3	725.1	727.8	727.0667	762.3221
30x30	725.5	725.3	726.5	725.7667	760.9591

APPENDIX IV.c Depth 15cm

field sizes	1	2	3	average	corrected readings
4x4	732.3	729.1	729.7	730.3667	765.7821
5x5	730.1	731.7	728.9	730.2333	765.6423
6x6	729.9	731.2	728.2	729.7667	765.1531
7x7	728.7	731.4	728.7	729.6	764.9783
8x8	726.7	728.8	728.4	727.9667	763.2658
9x9	727	728.5	726.3	727.2667	762.5318
10x10	726.2	728.8	725.6	726.8667	762.1124
12x12	725.6	727.3	727.9	726.9333	762.1823
15x15	726	726.8	725.5	726.1	761.3086
20x20	725.8	725.1	727.3	726.0667	761.2736
25x25	726.8	724.9	726.3	726	761.2037
30x30	726	725.6	726.2	725.9333	761.1338

APPENDIX –IV.d Depth 20cm

field sizes	1	2	3	average	corrected readings
4x4	742	742	740	741.3333	777.2806
5x5	742.3	741.6	739.6	741.1667	777.1058
6x6	743.4	741.4	734.9	739.9	775.7778
7x7	734.9	738.8	739.4	737.7	773.4711
8x8	734	735.9	738.5	736.1333	771.8284
9x9	737.1	735	734.9	735.6667	771.3391

10x10	736.6	736.1	730.3	734.3333	769.9412
12x12	733	733.1	735.2	733.7667	769.347
15x15	733.9	733.2	732.9	733.3333	768.8927
20x20	731.7	734.3	733	733	768.5432
25x25	736.9	734.9	725.5	732.4333	767.949
30x30	727.8	723.7	735.3	728.9333	764.2793

APPENDIX V TISSUSE AIR RATIO CALCULATION

APPENDIX IV.a Depth 5cm

field sizes	Tissue	Air	TAR
4x4	729.5915	762.4969	0.956845
5x5	728.9285	759.5262	0.959715
6x6	730.4989	759.2815	0.962092
7x7	730.6385	759.0019	0.962631
8x8	733.4304	757.8486	0.96778
9x9	733.7794	755.8564	0.970792
10x10	734.233	755.6817	0.971617
12x12	734.8612	754.7031	0.973709
15x15	735.0706	754.2837	0.974528
20x20	735.5592	750.1596	0.980537
25x25	736.1874	749.9849	0.981603
30x30	736.3619	749.88	0.981973

APPENDIX IV. b Depth 10cm

field sizes	Tissue	Air	TAR
4x4	713.3287	765.7122	0.931589
5x5	713.7824	765.5375	0.932394
6x6	713.3287	764.9783	0.932482
7x7	714.5502	764.7337	0.934378
8x8	716.0508	764.8735	0.936169
9x9	717.2723	765.0832	0.937509
10x10	717.2723	764.4541	0.93828
12x12	717.3421	764.3492	0.9385
15x15	719.2615	763.6153	0.941916
20x20	721.2507	762.6716	0.94569
25x25	721.5997	762.3221	0.946581
30x30	721.8673	760.9591	0.948628

APPENDIX IV .c Depth 15cm

field sizes	Tissue	Air	TAR
4x4	701.2538	765.7821	0.915735
5x5	702.5451	765.6423	0.917589
6x6	702.58	765.1531	0.918221

7x7	704.0108	764.9783	0.920302
8x8	708.0939	763.2658	0.927716
9x9	710.2926	762.5318	0.931492
10x10	711.4442	762.1823	0.93343
12x12	711.6536	762.1124	0.933791
15x15	713.0496	761.3086	0.93661
20x20	714.62	761.2736	0.938716
25x25	714.7247	761.2037	0.93894
30x30	717.5515	761.1338	0.94274

APPENDIX IV. d Depth of 20cm

field sizes	Tissue	Air	TAR
4x4	698.0082	777.2806	0.898013
5x5	701.6377	777.1058	0.902886
6x6	701.7773	775.7778	0.904611
7x7	703.3477	773.4711	0.909339
8x8	704.1155	771.8284	0.912269
9x9	704.6739	771.3391	0.913572
10x10	705.8604	769.9412	0.916772
12x12	707.2215	769.347	0.919249
15x15	708.408	768.8927	0.921335
20x20	711.3744	768.5432	0.925614

25x25	711.6187	767.949	0.926648
30x30	714.5153	764.2793	0.934888

APPENDIX V OFF AXIS MEASUREMENT AT VARIOUS WIDTH FROM THE CENTRAL AXIS IN nC

APPENDIX V.a depth 5cm

WIDTH (OFF AXIS READINGS ON THE LEFT)						CENTRAL AXIS READINGS	WIDTH (OFF AXIS READINGS ON THE RIGHT				
Field sizes	-5	-4	-3	-2	-1	0	1	2	3	4	5
4×4	615	627.7	638.2	650.7	662.4	696.6	644.9	629.3	610.5	576.7	549
5x5	615.3	627.7	638.7	650.9	663.1	696.2	644.9	629.1	609.1	576.7	547.2
6x6	616.7	628.1	638.7	651.3	664.9	697.7	644.3	629	608	575.2	546
7x7	617.1	628.9	639.9	651.4	665.3	697.9	643.7	626.3	607.6	574.9	545.1
8x8	617.9	630.3	640.2	652	666.7	700.5	642.1	624.8	605.4	573	544.4
9x9	618.5	630.9	640.8	652.4	667.2	700.9	641.4	623.1	603.7	572.4	543
10x10	620	631.7	641.5	654.7	668.5	701.3	640	622.9	602.5	569.9	540
12x12	621.9	632	642.7	655.9	670.4	701.9	639.2	621.1	601.9	567.3	536.5
15x15	622.7	632.3	643.9	656.4	673.4	702.1	637.4	620.3	601.1	565.5	534
20x20	623.5	634.1	644.4	658.9	674.9	703.2	637	619.1	600	564	532.9
25x25	624	634.9	645.7	660.4	676.1	702.6	636.8	618.3	600	563.2	530

30x30	624.5	635.2	646.5	661.8	678.6	703.3	635.1	616.4	598.9	562	528.3

APPENDIX V.b depth 10cm

WIDTH (OFF AXIS READINGS ON THE LEFT)						CENTRAL AXIS READINGS	WIDTH (OFF AXIS READINGS ON THE RIGHT				
Field sizes	-5	-4	-3	-2	-1	0	1	2	3	4	5
4×4	608.7	620.9	634	641.2	669	681.3	672.3	630.1	558.7	529	488.5
5x5	608.7	621.3	634.5	640.5	670.4	681.7	671.9	629.9	556.1	527.3	487
6x6	609.3	622	635	640.9	670.4	682.5	670.5	629.7	555	526.4	486.2
7x7	609.7	623.5	635	641.3	671.3	685.1	669.9	628.5	553.6	525	485.4
8x8	610.6	624.9	636.5	642	672.1	683.9	668.3	627.7	552	523.7	484.1
9x9	611	625.7	637.4	644.5	672.9	681.3	667	627	551	521.4	483.5
10x10	612.8	626	639.2	645.7	674	685.1	666.5	626.5	550.4	519.3	481.7
12x12	614.5	628.2	640.7	648.3	675.9	685.2	654.9	626.5	548.5	517.7	480.3
15x15	615.8	629.9	642.3	649.9	676.4	687	650.3	626.2	545.7	515	478.5
20x20	617.7	630.1	643.7	650.3	677.9	688.9	647.4	625.3	544	513.1	476
25x25	618	631.4	645.2	651	678.2	689.2	642.8	623.2	542.1	510.6	475.2
30x30	619.7	632	647.3	652.7	679.1	689.5	632.5	621.5	540.3	509.7	473

APPENDIX V.c Depth 15cm

WIDTH (OFF AXIS READINGS ON THE LEFT)						CENTRAL AXIS READING	WIDTH (OFF AXIS READINGS ON THE RIGHT				
Field sizes	-5	-4	-3	-2	-1	0	1	2	3	4	5
4×4	486.3	540.9	563	633.2	650.3	669.8	645.7	627.4	609.1	576.7	500
5x5	486.9	541.3	563.7	633.2	651.1	671	643.7	626	608	575.2	499.5
6x6	487.5	542	564.3	633.2	653	671.1	643.3	625.7	607.6	574.9	498
7x7	488.7	543.8	565.5	634.1	653.9	672.4	642.1	623.7	605.4	573	497.5
8x8	489.5	544.1	566.8	635.6	655.4	676.3	640.7	622.3	603.7	572.4	496.4
9x9	491.3	545.3	567.5	636.6	655.9	678.4	638.9	622.5	602.5	569.9	497
10x10	493.7	546.7	569	637.8	658.3	679.7	637.3	621.8	601.9	567.3	495.6
12x12	495.5	549.8	571.5	639.4	660.7	680.3	636.5	620	601.1	565.5	492.7
15x15	497.7	553.3	572.9	640.1	661.9	681.1	634	619.7	600	564	490
20x20	498.6	553.9	573.5	642.7	663.5	682.6	633.5	617.2	600	563.2	487.6
25x25	500.6	555.7	575.8	643.3	664.7	682.7	632.5	612.4	598.9	562	485.4
30x30	502.8	557.4	577.3	644.8	665.3	685.4	630.5	611.9	590.1	561	483

APPENDIX V.c depth 20cm

WIDTH (OFF AXIS READINGS ON THE LEFT)						CENTRAL AXIS READINGS	WIDTH (OFF AXIS READINGS ON THE RIGHT				
Field sizes	-5	-4	-3	-2	-1	0	1	2	3	4	5
4×4	484.4	553.7	578.2	628.4	647.7	666.7	672.3	654.2	534	549.7	501.7
5x5	485.9	553.9	578.9	628.5	647.9	670.1	671.9	653.7	616.3	547.4	499.7
6x6	486.7	554.3	579	628.5	648.1	670.3	670.6	652.9	615.9	546.7	499.2
7x7	487.5	555.9	580.4	630.1	649.7	671.8	669.5	652.1	614	545	497.5
8x8	489.2	556.8	581	630.9	650.2	672.5	668.1	650.4	612.7	544.4	494.8
9x9	490.5	558.3	582.1	632.4	651.9	673.1	667	649.9	609.8	543.5	492.5
10x10	491.7	560.1	583.4	633.7	652.3	674.2	665.3	645.7	607.3	542	490
12x12	492.6	561.9	584.1	634.8	653.9	675.5	664.1	643.9	605.7	540	487.3
15x15	493.3	562.6	586	636.9	654.3	676.6	662.3	642.1	604.9	539.7	485
20x20	495.7	567.5	588.3	638.4	655.8	679.4	660	641.3	603.5	537.9	483.2
25x25	498.9	568.7	589	640.1	656.4	679.7	659.7	640.1	602.7	535.6	482
30x30	501.5	571.2	591.3	642.9	657.2	682.5	658.1	639.2	601.8	534	480